BASIC HYDRODYNAMIC PROCESSES IN THE COASTAL ZONE

by L.C. van Rijn, www.leovanrijn-sediment.com, March 2013

1 Introduction

The coastal zone situated between the coastline and the shelf is the territory of winds, waves and currents. Usually, the coastal zone is subdivided in three zones:

- the **dune and beach** zone dominated by wind and wave forces;
- the **surf zone (upper shoreface)** dominated by breaking waves and wave-induced currents; under calm conditions the surf zone may be reduced to a narrow swash zone, but under storms it may extend offshore to depths of 8 to 10 m, where the waves first begin to break;
- the **middle and lower shoreface** zone dominated by non-breaking waves and tide-, density- and wind-induced currents.

The nearshore zone with depths up to 10 m is a **friction-dominated zone** with turbulent mixing of water; the lower shoreface zone with depths larger than 20 m is a **geostrophic zone** dominated by tide-, wind- and density-driven flows and affected by Coriolis forces (Ekman turning). In the geostrophic zone three vertical layers are present: surface boundary layer, interior layer and bottom boundary layer. In between the friction-dominated zone and the geostrophic zone a transition zone with characteristics of both adjacent zones can be distinguished.

Although considerable progress of our knowledge of coastal processes has been made during the last decade as a result of numerous field studies, many details of the near-bed hydrodynamics are still poorly understood.

The aim of this paper is to summarize the most important characteristics of the hydrodynamics in the coastal zone. **Figure 1.1** shows a schematic illustration of the processes involved (after **Wright et al, 1994**).

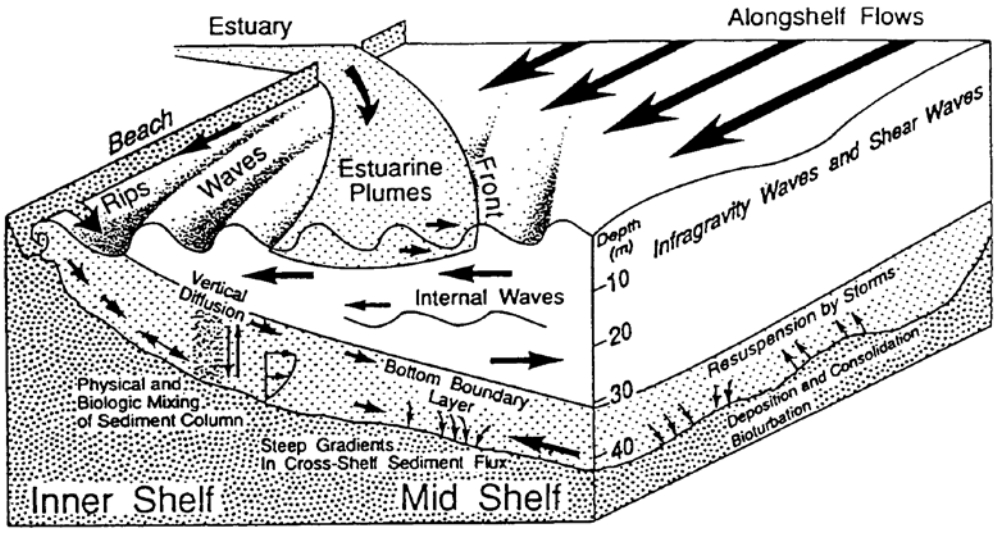

Figure 1.1 *Hydrodynamic processes in the coastal zone (after Wright et al, 1994)*

The main hydrodynamic processes in the coastal zone are:

- wind-induced and tide-induced waves,
- tide-, wind-, density- and wave-induced currents.

The wave phenomena in the shoreface zone are characterized by different types of motions on different types of scales. Basic wave motions associated with these scales are wind-waves and tides.

Wind-induced waves with typical periods of 5 to 15 seconds propagating into shallow water are affected by reflection, refraction, bottom friction and shoaling phenomena and finally by wave breaking in the surf zone. Especially in the shoaling phase before breaking, the wave profile is highly distorted associated with bound higher harmonics (wave asymmetry). Wave breaking inside the surf zone results in the generation of organized mean cross-shore and longshore currents as well as in the generation of chaotic high-frequency and small-scale turbulence.
The incident short waves carry a small forward mass flux inside the wave trough-crest region to the shore, increasing in magnitude through the breaking zone and finally piling up at the beach (set-up of mean water level). As a consequence of the presence of a cross-shore water surface gradient, a near-bed return current (undertow) is generated, balancing the onshore mass flux. Oblique incident waves also generate a longshore mean current. Very close to the bed in the wave-boundary layer onshore-directed streaming may occur due to an unbalance of the local fluid shear stresses.
Longshore variability of breaker bars may result in the generation of localized seaward-going currents, known as rip currents which are fed by the longshore currents. These rip currents spreading out in the deeper surf zone in combination with adjacent landward-going surface currents (mass transport) can be interpreted as horizontal circulation cells, moving gradually along the coast.

Low-frequency wave motions with periods in the range of 15 to 100 seconds have been observed outside and inside the surf zone, especially during rough weather conditions. Their importance is enhanced through the surf zone as a result of wave breaking (surf beat). Cross-shore and longshore wave propagation modes have been identified in the coastal zone. Cross-shore modes are associated with forced long waves which are bound to short wave groups or to long-period variations in the break locations of irregular short waves. Longshore low-frequency waves may be progressive or standing edge waves trapped in the surf zone.

Tidal waves have typical periods in the range of 12 to 24 hours; tidal motion is related to the gravitational interaction between the Sun, the Earth and the Moon. Tidal waves in coastal seas are originating from tidal forces generated in the deep oceans. Phenomena like reflection, refraction, bottom friction and shoaling affect the tidal waves during propagation to the shore resulting in variations of the tidal range and the generation of amphidromic systems. Wave damping by bottom friction and wave deformation due to differences in the crest and trough propagation speeds become more important in the shallow shoreface leading to wave asymmetry and phase differences between the vertical (surface elevation) tide and the horizontal (current) tide. Geostrophic forces related to the rotation of the Earth (Coriolis effect) are of importance in areas further offshore (lower shoreface, depths larger than 20 m).
In the nearshore zone the tidal currents tend to be shore parallel; the current vector rotates in a flattened elliptical pattern. Residual currents usually are small (order of 0.1 m/s) and may be enhanced by wind-induced currents, density-induced currents and by local topographical effects (islands, headlands, sand banks).

Besides tidal effects, there are also large-scale shoreface circulations, driven by wind-induced and density-induced forces with bottom friction as the main controlling parameter.

Wind blowing in a certain direction will induce currents in that direction and in various other directions due to Coriolis forces resulting in a spiral-type turning of the velocity vectors at different elevations above the bed, which is known as the Ekman spiral. In shallow water near the shore the currents respond rapidly to the wind stresses and tend to be aligned with the wind direction. The shore-normal component of the wind stress and the related surface current causes a set-up (or set-down) of the water surface at the shore. As a consequence, a cross-shore pressure gradient is generated yielding an onshore (or offshore) bottom current.

Longshore winds and associated longshore currents also induce cross-shore currents by the action of Coriolis forces yielding a set-up or set-down of the water surface near the shore and corresponding cross-shore bottom currents, depending on the wind direction.

Density-induced currents are related to spatial density gradients of the fluid-sediment mixture due to variations of the salinity, temperature and/or sediment concentration. Usually, the fluid density related to salinity variations is decreasing in landward direction as a result of river (fresh water) outflow. The density-gradient effect is most pronounced in the near-bed region yielding relative large onshore near-bed velocities during the flood tide and relatively small offshore velocities during the ebb tide. As a consequence a near-bed residual current (landward) is generated, which may cause a net landward transport of sediments.

2 Wind-induced waves

Incident waves coming from the sea to the shore can be divided into three categories:

- wind waves and swell; these are the most energetic and readily visible waves;
- bound long waves; these are long waves associated with modulations in the wind waves and are travelling at the group velocity of wind waves; regions of high waves carry along a depression of the mean water surface level, known as "set-down";
- free long waves; edge waves may be incident from the adjacent coastal regions.

2.1 High frequency waves

Waves moving in a wind field will be propagated in the main wind direction. As a result of the variability of the wind forces the sea surface shows a large variety of waves moving with different frequencies, phases and amplitudes. Often, there are coherent groups of high and low waves. Waves moving out of the wind field become more regular and symmetric (sine waves) with relatively long crests and are known as swell waves.
The near-bed peak orbital velocity of a sine wave is described by linear wave theory: $U_\delta = (\pi H)/(T \sinh(2\pi h/L))1$ in which: $U_\delta 2$ = peak orbital velocity at edge of boundary layer, H = wave height, T = wave period, h = mean water depth, L = wave length. Maximum values of the peak orbital velocity in shallow water under storm conditions are of the order of 2 to 3 m/s.

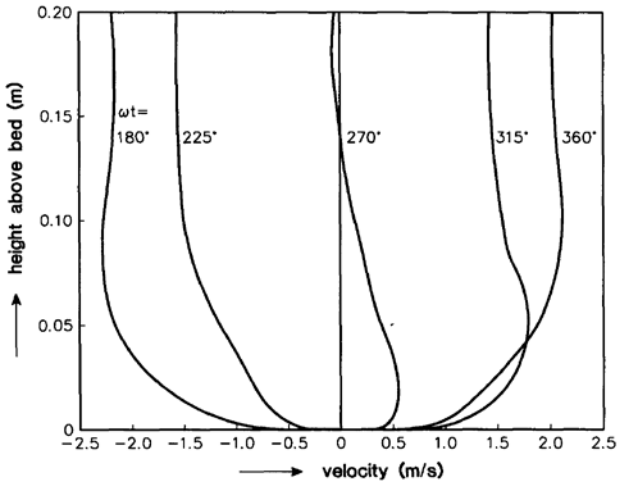

Figure 2.1 *Velocity profiles in wave boundary layer*

The layer between the location of the peak near-bed orbital velocity (U_δ3) and the bottom (zero velocity) is known as the wave boundary layer. **Figure 2.1** shows instantaneous velocity profiles (within wave cycle) of the wave boundary layer over a rough bottom.

Waves play a dominant role in the nearshore zone. Wave processes are responsible for large oscillatory fluid motions which drive currents, sediment transport and bed level changes.
During its propagation to the shore, the relatively well-organized motion of offshore waves is transformed into several motions of different types and scales, including small-scale turbulence, large-scale coherent vortex motions and oscillatatory low-frequency wave motions.
Waves entering shallow water are subjected to: shoaling, refraction, reflection, diffraction, bottom friction and breaking.

Shoaling and breaking waves become asymmetric (peaked crests and wide troughs, see **Figure 2.2**) resulting in larger onshore-directed velocities under the wave crest and smaller offshore-directed velocities under the wave trough. The asymmetry increases with increasing relative wave height (H/h), which is of fundamental importance with respect to the net onshore-directed transport processes causing accretion of beaches. **Figure 2.3** shows the significant wave height ($H_{1/3}$), the fraction of breaking waves and the asymmetry of the shoaling waves over a breaker bar in a laboratory experiment (**Grasmeijer and Sies, 1995**). The asymmetry factor is defined as $A_1 = U_{s,on}/U_{s,off}$ 4with $U_{s,on}$5 = significant near-bed onshore peak orbital velocity and $U_{s,off}$6 = significant near-bed offshore peak orbital velocity. As can be observed, the asymmetry is largest just seaward of the crest of the bar.

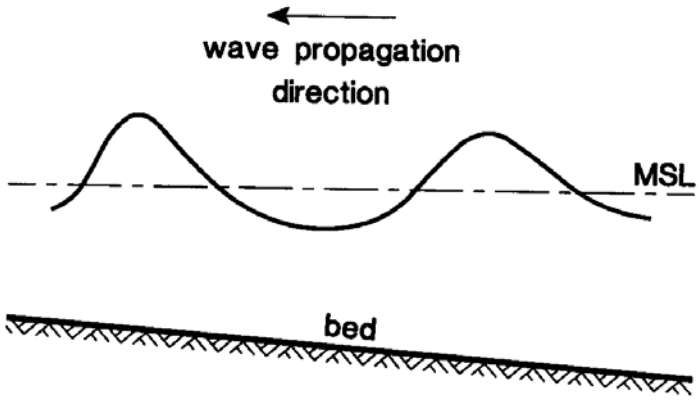

Figure 2.2 *Wave profile of shoaling waves*

Information of the asymmetry of the near-bed peak velocities based on field data of the Dutch coastal zone is given in **Figures 2.4** and **2.5** (**Houwman and Hoekstra, 1994; Kroon, 1994**).
The asymmetry is defined as $A_2 = U_{s,on}/ (U_{s,on} + U_{s,off}$ 7).
In water depths larger than about 7 m the asymmetry remains relatively small with maximum values of about 0.55 under storm conditions $U_{s,on}$ =1.2 $U_{s,off}$ 8.
In the shallow surf zone the maximum asymmetry value is 0.65 under plunging waves $U_{s,on}$ =1.5 $U_{s,off}$ 9.
Many higher-order wave theories are available to determine the asymmetry of the near-bed velocities. The most popular wave theories are based on the assumption of potential flow over a flat bed.
Analytical solutions have been derived by making expansions in a small parameter yielding solutions up to the 5th-order for deep water (Stokes-solutions) and shallow water (Cnoidal-solutions).
Numerical methods based on Fourier approximations give solutions in the form of truncated Fourier series (**Sobey and Bando, 1991**; **Rienecker and Fenton, 1981**).

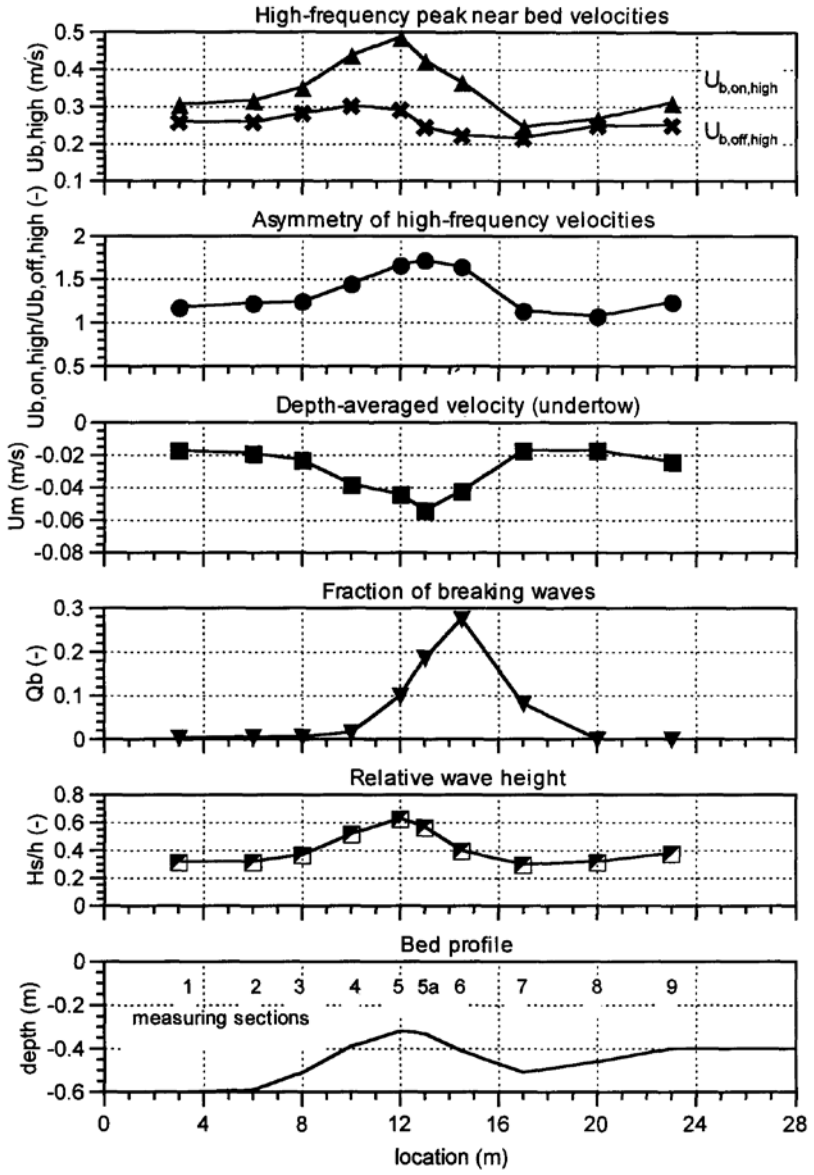

Figure 2.3 *Asymmetry of near-bed peak orbital velocity along a breaker bar profile in case of a laboratory experiment*

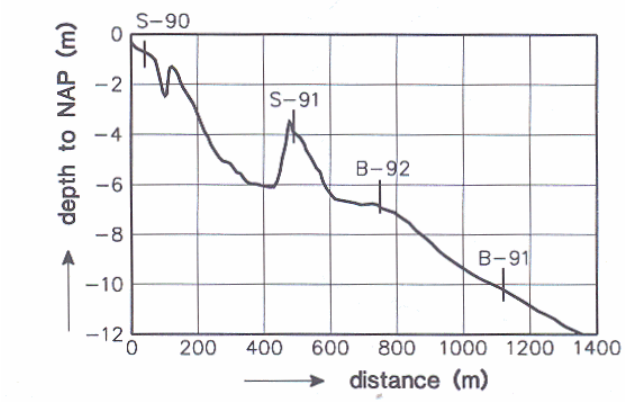

Figure 2.4 *Measurement stations in a cross-shore profile near Egmond, The Netherlands*

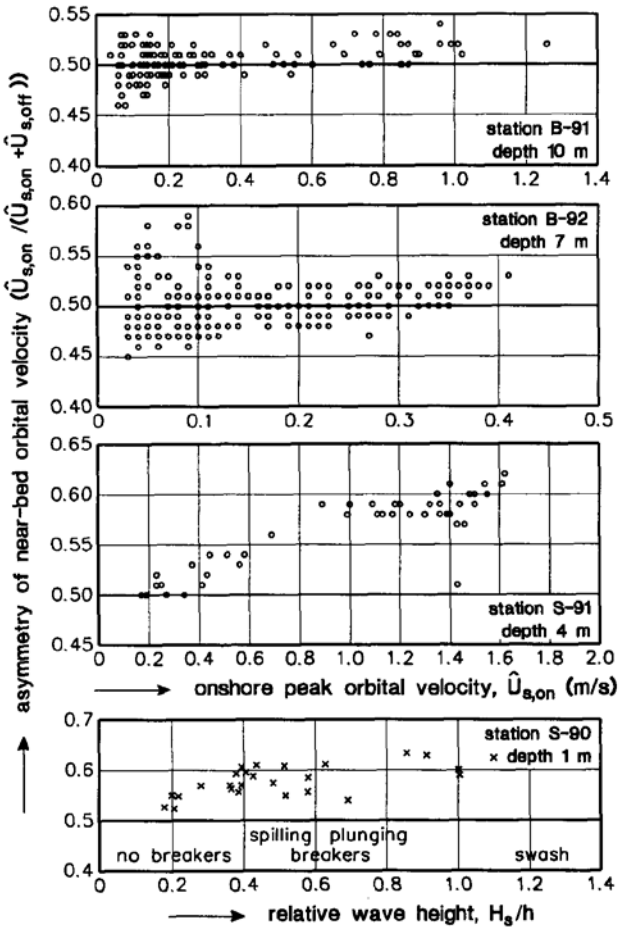

Figure 2.5 *Asymmetry of near-bed peak orbital velocity in four stations (see Fig. 2.4)*

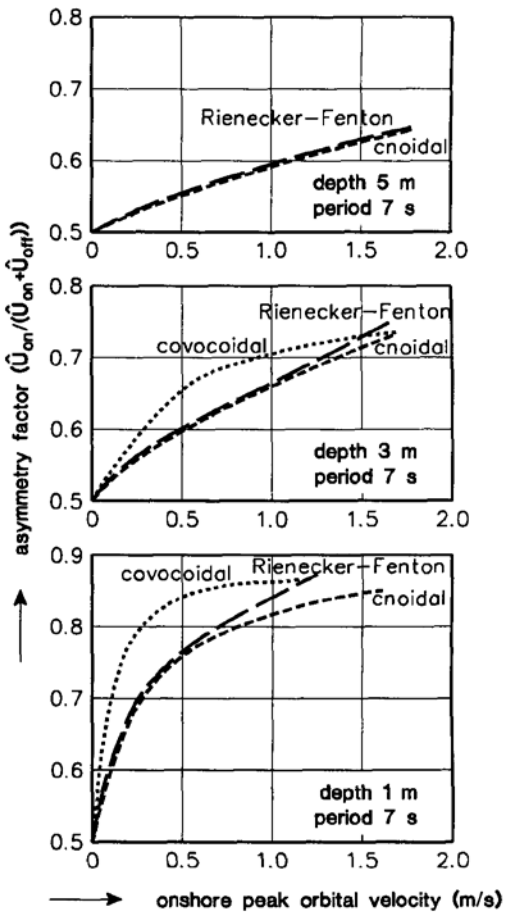

Figure 2.6 *Asymmetry factors*

Parameterized solution methods based on an empirical wave shape for any depth over a horizontal bottom (Vocoidal theory) and later over a sloping bottom (Covocoidal theory) have been introduced by **Swart and Loubser (1978)** and **Swart and Growley (1988)**.
A recent development is the representation of non-linearity in the incident short waves by modelling the full wave motion. Outside the breaking zone Boussinesq equations provide an accurate modelling of the non-linear transformation of irregular wave trains including wave-wave interaction and the propagation of bound long waves.

Figure 2.6 shows asymmetry factors of three wave theories in water depths of 5, 3 and 1 m for a wave period of 7 s. In case of a depth of 5 m the three methods produce similar results. For a depth of 3 and 1 m the *Cnoidal* theory and the *Rienecker-Fenton* Fourier approximation theory yield similar results; the *Covocoidal* theory gives significantly larger values. Compared to asymmetry factors for field conditions (maximum asymmetry A_2 of about 0.65 in shallow water, see **Figure 2.5**), the applied wave theories produce relatively large values, especially in shallow water and even for low orbital velocity values (low waves).

Waves start to break when the fluid velocities of the wave crest tend to become equal to the wave propagation velocity. Wave breaking mainly occurs in the surf zone and is strongly related to the presence of bars.

Three main types of breaking waves are distinguished, depending on the beach slope and the wave steepness:

- spilling breakers,
- plunging breakers,
- surging breakers.

Spilling breaking is dominant in case of high wave steepness and mild bottom slopes, whereas plunging breaking is dominant in case of low wave steepness and steep bottom slopes.
The maximum wave height according to linear wave theory is about 0.8 of the local water depth for a horizontal bed (H_{br}= 0.8 h). Laboratory experiments with regular waves show however maximum wave heights of about 0.5 times the depth (H_{br}= 0.5 h) over a horizontal bottom up to values of 1.2 times the water depth (H_{br}= 1.2 h) over steep bottom slopes (**Nelson, 1983; Weggel, 1972**). In general, random waves break with smaller wave heights than regular (monochromatic) waves as most of the waves break on opposing flows due to generated long wave components or rip currents (**Sato et al, 1990**).
The onset of breaking of irregular waves appears to be about H_s/h=0.3 to 0.4.

Four distinct breaking wave classes were found by **Kroon (1994)** in the surf zone:

- non-breaking waves $H_s/h \leq 0.4$
- spilling breaking waves $H_s/h > 0.4$ and ≤ 0.6
- plunging breaking waves $H_s/h > 0.6$ and ≤ 0.9
- surging/plunging breaking waves (swash zone) $H_s/h > 0.9$

Figure 2.7 shows an example of the wave height decay (H_{rms}) due to breaking in a cross-shore profile with two breaker bars according to a probabilistic wave model (**Van Rijn and Wijnberg, 1994, 1996**). The cross-shore distribution of the water level set-up is also shown.

Wave breaking and associated energy dissipation play an essential role in the surf zone dynamics because these processes result in gradients of the radiation stresses driving the set-up of the mean water level and the longshore currents.
The surf zone shoreward of the breaking point can be roughly divided in three subzones (**Svendsen, 1984**): outer breaking zone, inner breaking zone and swash zone.
In the **outer breaking zone** the breaking waves are transformed into turbulent bores with a rapid transition of the wave shape including the generation of a surface roller. Most of the potential energy lost in breaking is converted into kinetic energy of organized large vortices.

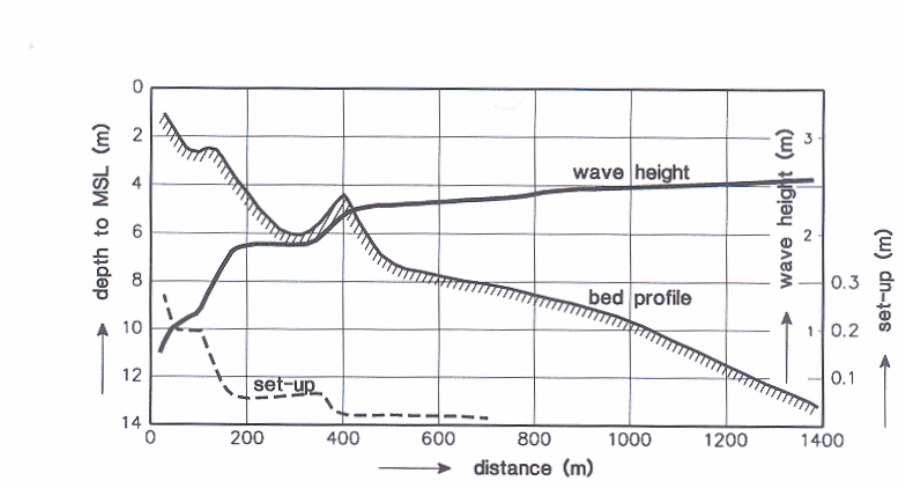

Figure 2.7 *Wave height and set-up for a barred profile*

In the **inner breaking zone** the kinetic energy of the organized vortex and roller motions is dissipated into small-scale turbulent motions. Longshore currents, cross-shore return currents and mean water level set-up are generated. The process of energy transfer causes a lag between wave breaking and the generation of mean flow, especially in case of a barred bed profile.

In the **swash zone** near the shoreline the water motion is characterized by the up- and downrush of plunging breaking waves in combination with low-frequency oscillations. The vertical distance between the water line at downrush and at uprush is termed the swash height (R). Generally, the long-period oscillations at the shoreline are dominant. The low-frequency swash height (R_{lf}) is found to be linearly related to the significant short wave height at the breaker line: $R_{lf} = 0.7\ H_{s,hf,br}$ for beaches of low slopes (**Huntley et al., 1993**).

For a wide barred surf zone along the North Sea (The Netherlands), **Ruessink (1998)** found a strong increase of the lf swash height with increasing offshore wave height. The high frequency swash height was found to vary weakly with offshore wave height (saturated conditions).
Some values are:

- R_{hf}= 0.2 m and R_{lf}= 0.2 m for $H_{s,0}$= 0.5 m,
- R_{hf}= 0.4 m and R_{lf}= 1 m for $H_{s,0}$= 5 m.

The results can be expressed as: $R_{lf}= 0.17 + 0.18\ H_{s,0}$ with $H_{s,0}$= significant offshore wave height (in m).

The results can also be related to the surf similarity parameter: $R_{lf}= 0.65\ H_{s,0}\ \tanh(3.4\gamma_0)$
with $\gamma_0= \tan\beta/(H_{s,0}/L_{s,0})^{0.5}$ and $\tan\beta$= beach slope.

Results of other researchers for different coasts have been summarized by **Ruessink (1998)**

Plunging breakers are characterized by a large-scale curling of the wave with an inner air core and a falling jet impacting on the oncoming trough. When the jet starts forming, the pressure under the wave crest remains less than hydrostatic because of the vertical accelerations. The curling of the wave crest implies a loss of potential energy that is transformed in kinetic energy when the water falls and contributes to the formation of vortices. The loss of wave energy has been seen to take place indirectly, through a repeated process of formation of discrete large-scale vortices. The vortices decay in smaller scales and dissipate their energy in turbulence. The turbulence generated by vortices does not remain confined near the surface, but spread downward and does not follow the wave crest. In the final stage the plunging breaker behaves like a bore and the wave undergoes the same evolution of the spilling breakers.

2.2 Low frequency waves

Interaction of all incident wind-waves with bed topography, with wave-generated and other currents in the nearshore zone generates long period motions. The long period motions can be subdivided into low-frequency waves (LFW) and vortical motions, such as present in longshore currents and rip currents. The term "infragravity waves" is also used to describe LFW, but since LFW are essentially gravity waves "infragravity" seems inappropriate. On a plane beach, the LFW motion is often described and analysed in terms of certain modes of motion, like edge wave modes and reflective or "leaky" modes. The only free modes are those corresponding to waves coming into the beach and being reflected there.
A review of LFW is given by **Hamm et al (1993) and Roelvink (1993)**. A summary of their review is given below.

All observations indicate that long period motions are caused by short waves incident on the coast. The major process involved is also clear. Short waves loose much or all of their energy by breaking. This dissipation differs strongly in its effects from the more commonly studied dissipation of fluid flows by frictional drag effects at

boundaries. Breaking usually leads to little or no internal fluid shear stresses and hence there is little or no loss of momentum. Momentum is carried into the surf zone by the short waves, driving both LFW and vortical motions. It is best formulated in terms of the momentum flux tensor, which is usually described as "radiation stress".

In the simplest case of a uniform short-wave train normally incident on a plane beach, there are no mean currents and the progressive transfer of momentum from the short waves breaking in the surf zone balances the pressure gradient due to wave-induced set-up of the water level. Any variation from non-uniformity in the incident wave train may lead to the generation of long wave motion.
The simplest case is that of free long waves. These are normally sufficiently small in amplitude that near-perfect reflection can be expected. However their interaction with the incident short waves may be quite significant. During half the long wave period, the short waves are "compressed" and during the other half they are expanded. Thus, the dissipation of their energy, and hence the transfer of momentum, is modulated in space and time by the long waves.

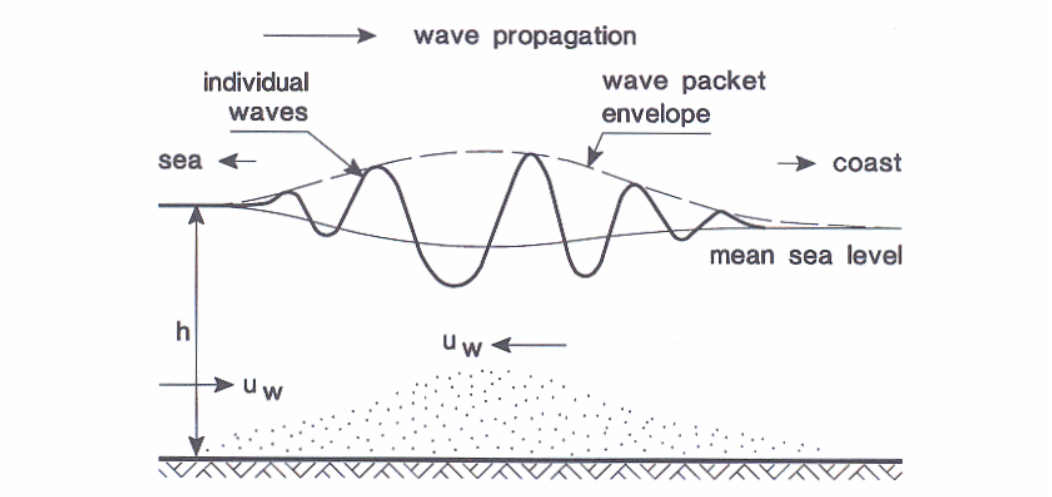

Figure 2.8 *Bound long waves*

Offshore there is a bound long wave accompanying such modulations **(Longuet Higgins and Stewart, 1964)**. These long waves with the crest under the low wave group and the trough under the high wave group (**Figure 2.8**) travel at the propagation velocity of the wave groups (group velocity) as bound long waves and may be released as free waves when the wave groups are destroyed, e.g. by wave breaking in the surf zone. The free waves are generally reflected on the beach and either escape to deep water ("leaky modes") or are trapped in the surf zone by refraction (edge waves). The long waves travelling on the time scale of the wave group period are also known as "surf beat". A clear discussion of bound long wave phenomena is given by **Roelvink (1993)**.

The presence of bound long waves can be shown by plotting the correlation between the short wave envelope curve and the long wave elevation for different time lags. The correlation should be of the order of -1 (at zero time lag) to explain low-frequency waves as bound long waves related to wave groups.

Figure 2.9 shows correlation values of about -0.5 in storm conditions at water depths of 7 m **(Houwman and Hoekstra, 1994)**, indicating that bound long waves are present. Similar correlation coefficients (-0.5) were obtained for conditions with relatively high waves in a water depth of 10 m. Correlation coefficients of the order of -0.5 indicate that bound long waves are present but do not fully dominate the infra-gravity band.

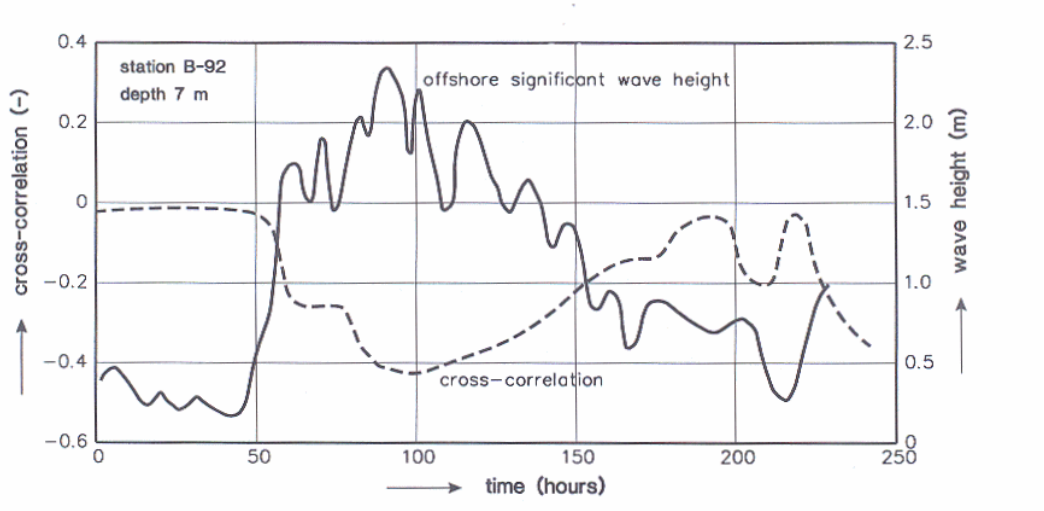

Figure 2.9 *Cross-correlation between wave envelope and low-frequency pressure in station B-92 (Fig. 2.4) near Egmond, The Netherlands*

Ruessink (1995, 1998) studied the behaviour of LF-waves in a cross-shore profile with multiple bars on the west coast of the island of Terschelling in the North Sea (The Netherlands). Tidal range varied between 1.2 and 2.8 m. Outside the surf zone the onshore propagating LF-waves were found to be dominated by bound long waves. Inside the surf zone these bound long waves were released as free waves. After refection at the shoreline, the LF-waves propagated back to deeper water. No evidence was found of breakpoint-forced long waves, both for normal incident as well as oblique incident short waves.

Another forcing mechanism generating long waves is the temporal and spatial break-point variation when the individual waves of the group break at the edge of the surf zone. Each time a wave breaks it generates a wave set-up localised within the zone of wave breaking, which can be seen as a local hump in the mean sea level. During storm conditions with multiple breaking zones this creates a long-period water oscillation (surf beat). The break-point moves back and forth; in this region there is a radiation stress gradient varying in time. In the break-point variation zone this radiation stress gradient varying in time acts as a local forcing mechanism (comparable to a wave maker in a laboratory basin) resulting in onshore and offshore-directed wave propagation.

Figure 2.10 shows a schematic representation of the wave height and set-up through the surf zone for a plane sloping beach face; x_1 and x_2 denote the minimum and maximum positions of the break point, as given by **Symonds et al (1982)**.

They studied breakpoint-forced long waves for a 2D-case and **Lippmann et al (1997)** for a 3D-case.

If the incident wave groups are very long, the set-up may adjust to the steady state conditions and the variation about the mean is denoted by Δs with a frequency about equal to that of the wave group. Time dependence phenomena will be significant for relatively short wave groups. The mean water level variation at position x_1 (at group frequency) generates long waves and its harmonics at the group frequency in both shoreward and seaward directions. The waves that propagate shoreward will be reflected at the shoreline and interfere with the offshore directed wave which may result in a standing wave pattern inshore of the forcing region. The waves that propagate seaward are outgoing progressive waves. The amplitude of long waves in the surf zone can be enhanced significantly if resonance conditions occur by wave trapping between the location of the breaker bars and the beach.

If the groupiness of the short waves persists into the surf zone, this will also cause low-frequency oscillations by the rising and falling mass of water at the shoreline (modulation of wave set-up) on the time scale of the wave groups.

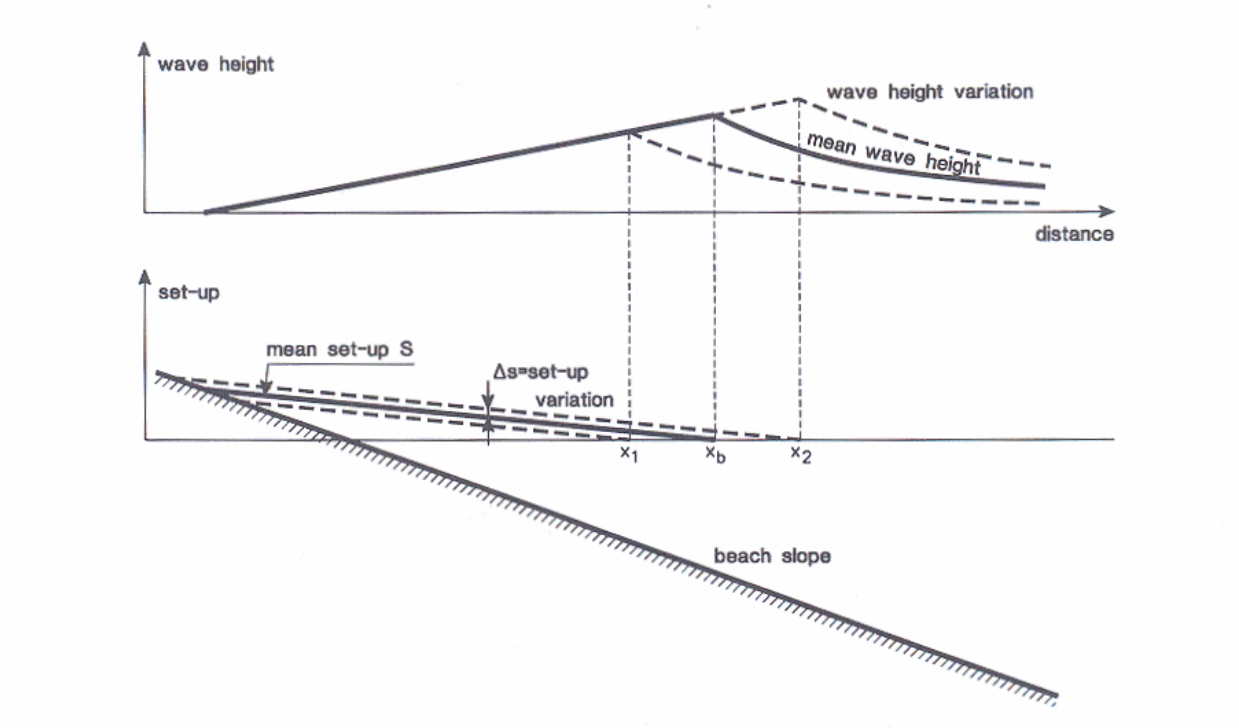

Figure 2.10 *Long wave generation by time-varying break point*

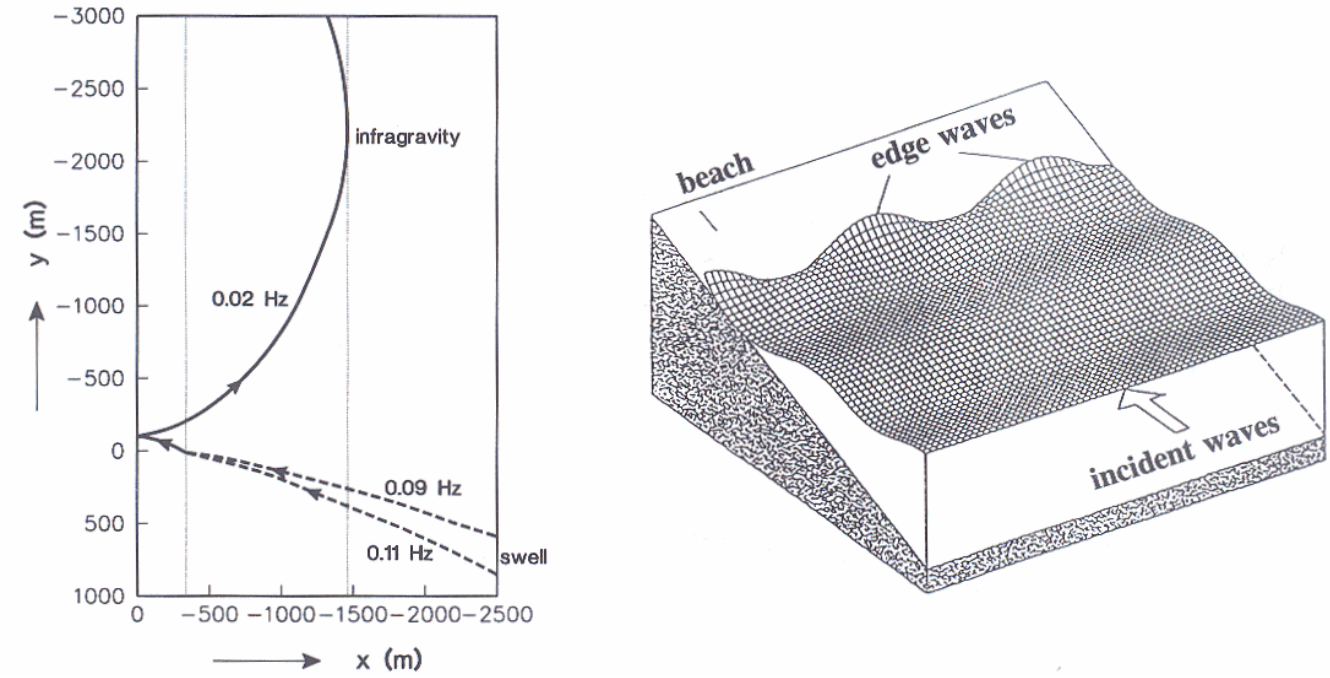

Figure 2.11 *Wave trapping and edge waves*
Left: Wave trapping
Right: Edge waves

Long waves generated by obliquely incident wave groups can be trapped in the nearshore zone by refraction. This can be demonstrated by an example **(Ruessink, 1998)**. Non-linear interaction of a pair of short waves with frequencies and wave numbers (f_1, k_1 and f_2, k_2) excite a bound wave with frequencies and wave numbers f_2-f_1, k_2-k_1. Suppose that at a depth of 4 m a free long wave is released by the breaking of two short waves with frequencies and directions (0.09 Hz, 25°) and (0.11 Hz, 30°). Their cross-shore and longshore wave numbers are (0.0846, 0.039) and (0.0987, 0.057). The frequency and wave numbers of the released (former bound) free wave are (0.02 Hz, 0.0151 in cross-shore direction and 0.018 in longshore direction), which corresponds to an angle of propagation of the free long wave at the moment of release of 50 degrees. This release angle is much larger than the incidence angles of the short waves. In case of a gently sloping wide surf zone the released free wave may easily be trapped, see **Figure 2.11**.

The resulting wave patterns are known as edge waves, see **Figure 2.11**. Edge waves can be described as cross-shore standing wave patterns propagating in longshore direction. **Ursell (1952)** has shown for a plane sloping beach that a discrete number of edge-wave modes and longshore wave numbers are possible for a given frequency; the number of zero crossings in cross-shore direction is given by the mode number. The amplitude envelope decays exponentially in offshore direction. Resonant excitation of edge waves by wave groups is possible if the forcing has an alongshore wave number corresponding with one of the edge wave modes at the group frequency.

For beaches bounded by headlands or by an entrance to a bay, standing edge waves corresponding to the modes fitting the beach length are the most likely to be observed. On long uniform beaches progressive edge waves may be more likely to occur but standing edge waves may also occur.
The overall effect (all components) of low-frequency cross-shore velocities in the inner surf zone is quite significant, as shown in **Figure 2.12**.

The ratio $U_{peak,lf}/U_{peak,hf}$ is about 0.1 to 0.2 (**Figure 2.12**) at low wave heights increasing to about 0.5 at high wave heights. Low-frequency velocities were found to be dominant under plunging breaking waves in the swash zone **(Kroon, 1994)**.

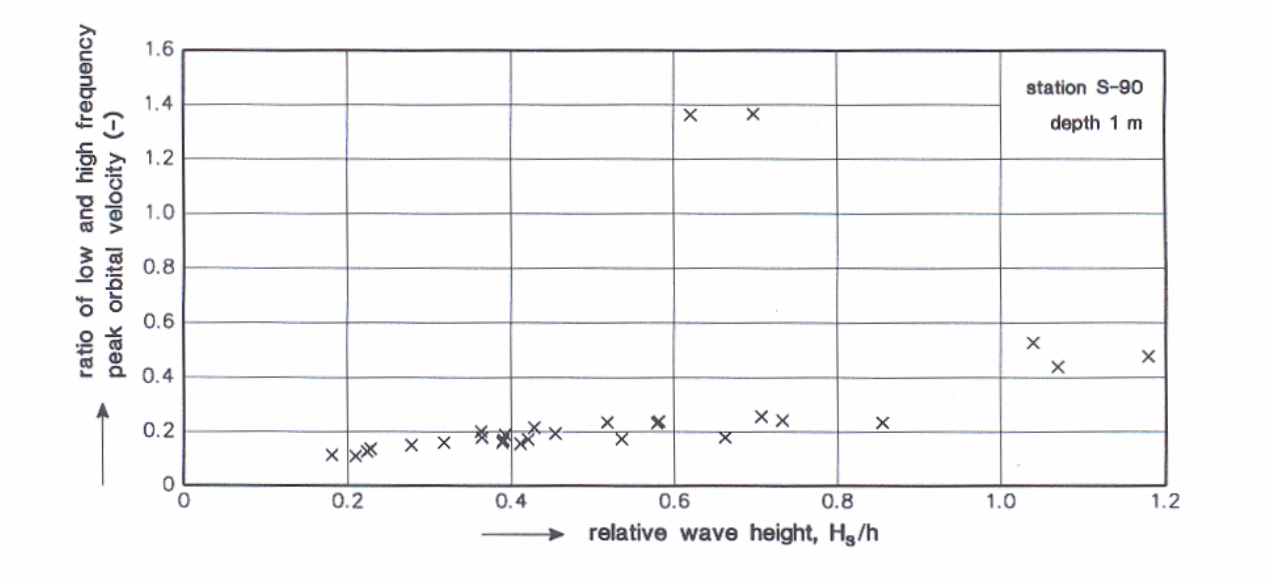

Figure 2.12 *Ratio of low-frequency and high-frequency peak orbital velocity in station S-90 (inner surf zone, Figure 2.4) near Egmond, The Netherlands*

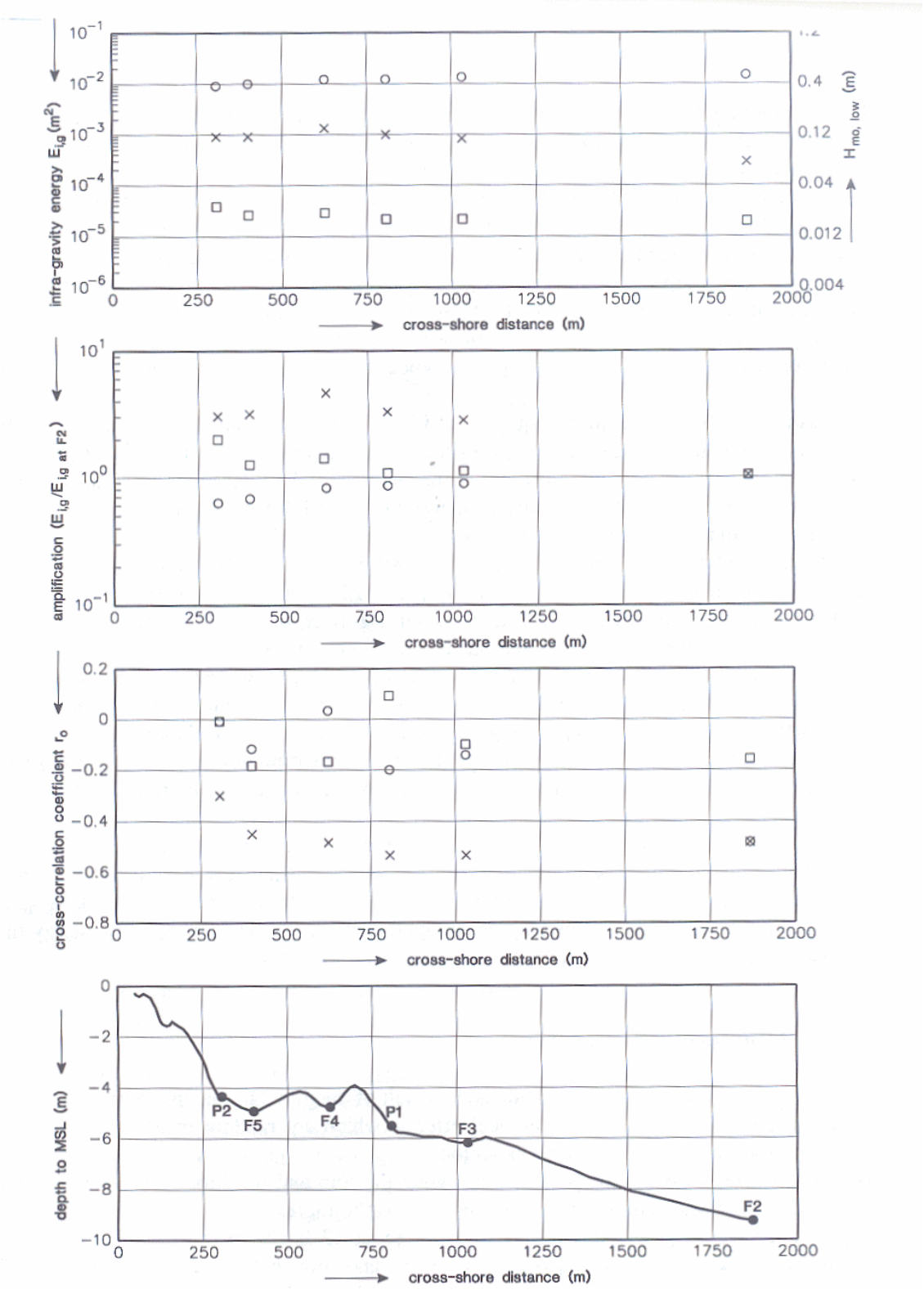

Figure 2.13 *Cross-shore change in infra-gravity energy for three events,Terschelling (o=high energy, x= moderate energy event, ☐= low energy event)*
Top: Infra-gravity energy
Middle: Amplification of energy with respect to location F2
Middle: Correlation of short wave envelope and long wave at zero time lag; large negative value is indication of bound long wave
Bottom: Cross-shore profile

Beach and Sternberg (1987) conducted a field experiment in the inner surf zone at San Marine, Oregon (USA) in October 1984 during conditions with offshore significant wave heights of 3 to 5 m (periods of 12 to 14 s). Tidal range was about 2.2 m. The beach had a slope of 1 to 30 and was composed of fine sand of 0.23 mm. Two longshore bars were present; the innermost of which was approximately 300 m offshore. The surf zone width was about 800 m. The instruments (electromagnetic current meters and OBS-optical sensors) were deployed at 70 m from the mean high water line (depth of 1.3 m). They observed events (duration of 30 min) with strong low frequency motion with wave height of about 1.2 m, period of about 100 s and peak orbital velocities of 1.5 m/s, superimposed by hf-waves of 0.8 m high. The offshore-directed lf-velocities corresponded to decreasing lf-water levels indicating a cross-shore standing wave pattern.

Ruessink (1998) studied low-frequency motions at the dissipative coast of Terschelling (The Netherlands) using pressure recordings at six cross-shore positions during October-November 1995. Two or three breaker bars were present at the field site. The tidal range was between 1.2 and 2.5 m. The short wave height ($H_{s,0}$) varied between 0.15 and 4.5 m.
Figure 2.13 shows the cross-shore profile and measurement positions and the cross-shore distribution of the infra-gravity energy (for three events) in the frequency band of 0.004 to 0.04 Hz. The lf-wave height is defined as $H_{mo}= 4E^{0.5}$ with E= spectral energy, see **Figure 2.13**.
Results of three events are shown:

- low-energy event, $H_{s,lf}$=0.02 m (□); infra-gravity levels are extremely low; bound long waves are absent as the correlation (at zero time lag) between the short wave envelope and the total low wave motion is almost zero; hence free long waves are dominant;
- moderate energy event, $H_{s,lf}$= 0.1 m (x); higher waves start to break on the middle bar between P1 and F4; bound long waves are dominant as correlation values are quite high; infra-gravity energy is strongly amplified in onshore direction (max. amplification=5 at F4); decrease of energy from F4 to P2 most probably because of bottom friction and breaking effects;
- high energy event, $H_{s,lf}$= 0.5 m (o); breaking of short waves seaward of F2; bound long waves are almost absent (released as free waves under breaking conditions); infra-gravity energy decreases in onshore direction because of bottom friction and breaking (as bores).

It can be concluded that at a low-sloping dissipative shoreface the infra-gravity energy in the form of bound long waves is maximum at the onset of short wave breaking.

3 Tide-induced currents

The generation of the astronomical tide is the result of the gravitational interaction between the Sun, the Earth and the Moon. Meteorological effects, which are random in occurrence, are generally superimposed on the tidal wave propagation.
The tidal range is maximum (spring tide) when the Sun and the Moon are in line and minimum (neap tide) when the Sun and the Moon are at a right angle.
Tidal waves are long waves with a period of about 12 hours in most places; in some places a dominant period of 24 hours can be observed. The propagation of tidal waves is affected by shoaling due to geometrical effects, by damping due to bottom friction, by reflection against boundaries and by deformation due to differences of propagation velocities under the wave crest and wave trough.
Tides are generated in oceans where the gravitational force due to the astronomical effect is most effective, resulting in a tidal range of the order of 0.5 m. The tidal currents in the deep ocean are extremely small (order 0.05 m/s).
The rotation of the Earth introduces an apparent force (Coriolis force) acting on the fluid. This force is significant in oceans, seas, wide estuaries and large lakes. The force is directed perpendicular to the direction of

the fluid motion (to the right on the northern hemisphere and to the left on the southern hemisphere). Areas where the Coriolis forces are significant, are known as geostrophic areas.

Tidal waves in coastal seas with depths ranging from 200 m offshore to 10 m nearshore are originating from tidal waves generated in the oceans. A long wave approaching the shelf area from the ocean will be partly transmitted on the shelf and partly reflected back to the ocean. The wave propagation direction will be changed at the shelf edge due to refraction effects. Shoaling will occur on the shelf, yielding a significant increase of the wave height on the shelf. The most important effect on the shelf is reflection of the tidal wave against the land boundaries. Reflection and Coriolis effects give rise to the generation of amphidromic systems (tidal wave rotating around a point with constant water level). Wave damping and deformation are important in shallow nearshore areas resulting in wave asymmetry and in phase differences between the horizontal (current) and vertical tide (elevation).

Tidal currents are controlled by:

- pressure gradients (mean surface slope, fluid density variations),
- bottom friction (dominant in depths smaller than 10 m),
- Coriolis forces (less important in depths smaller than 10 m).

Depth-averaged peak tidal velocities are of the order of 1 m/s at the seaward boundary of the shoreface zone and of the order of 0.1 m/s near the surf zone. Close to the shoreline the currents tend to be shore parallel and relatively unaffected by Coriolis forces. The current vector rotates in a flattened elliptical pattern. Tide-related residual currents (non-closed ellipse) usually are small (order of 0.1 m/s) and may be enhanced by density-induced currents, by wind-induced currents or by local topographical effects (islands, headlands, sand banks).

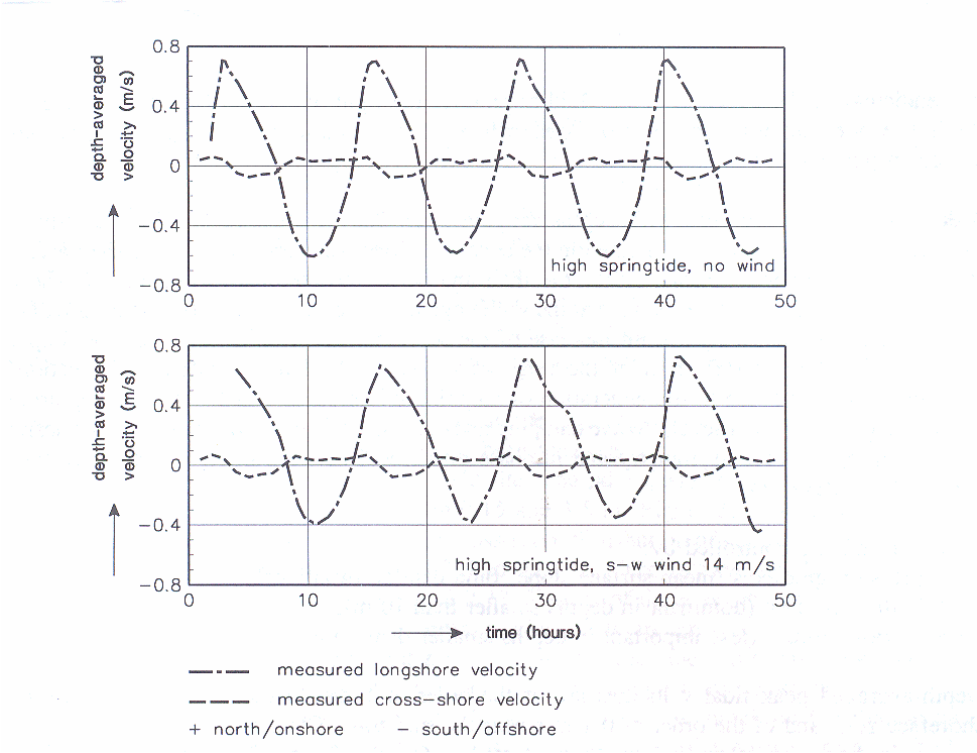

Figure 3.1 *Depth-averaged tidal current velocities in an offshore station (depth = 20 m), Noordwijk, The Netherlands.*
Top: wind velocity less than 5 m/s,
Bottom: wind velocity of 15 m/s (in flood direction)

Van de Meene (1994) concluded that the residual currents at the shoreface-connected ridges near Zandvoort in the North Sea (The Netherlands) are the result of a very delicate balance between tide, wind and density-induced effects, especially in cross-shore direction. The balance appeared to be very sensitive to varying hydrodynamic and meteorological conditions. His observations showed that close to the bed the onshore-directed density effect is dominant most of the time. Only during very strong onshore winds an offshore-directed residual current was observed.

Figure 3.1 shows an example of semi-diurnal depth-averaged tidal velocities in a station (Noordwijk) offshore the Dutch coast. The velocities were measured by use of an Acoustic Doppler Current Profiler at 17 elevations from 1 m above the bed to 1 m below the surface in water depths of approx. 20 m, **(Groenendijk, 1994)**. The peak longshore velocities during the spring flood tide (northward) are about 0.8 m/s and about -0.6 m/s during the spring ebb tide (southward), see **Figure 3.1**. The peak cross-shore velocities are about 0.1 m/s. During conditions with strong winds (15 m/s) from the south, the (southward) ebb current velocities are reduced and the (northward) flood current velocities are enhanced (see **Figure 3.1**) resulting in a more asymmetrical tidal curve and hence larger residual current velocities. In cross-shore direction the current velocities are mainly seaward directed during strong winds from southwest (**Figure 3.1**). The effect of the wind on the magnitude and direction of the longshore tidal velocities is even stronger in stations closer to the shoreline (less deep water), as can be observed in **Figure 6.8**.

4 Wind-induced currents

Two types of wind-induced currents can be distinguished:

1. wind drift currents of relatively short duration generated by local storm winds;
2. large-scale circulation systems generated by long duration effects such as trade winds, zonal winds, atmospheric pressure systems (Gulfstream, Florida current, Equatorial currents).

In deep water the vertical structure of the wind-induced velocity profile is shown in **Figure 4.1**.

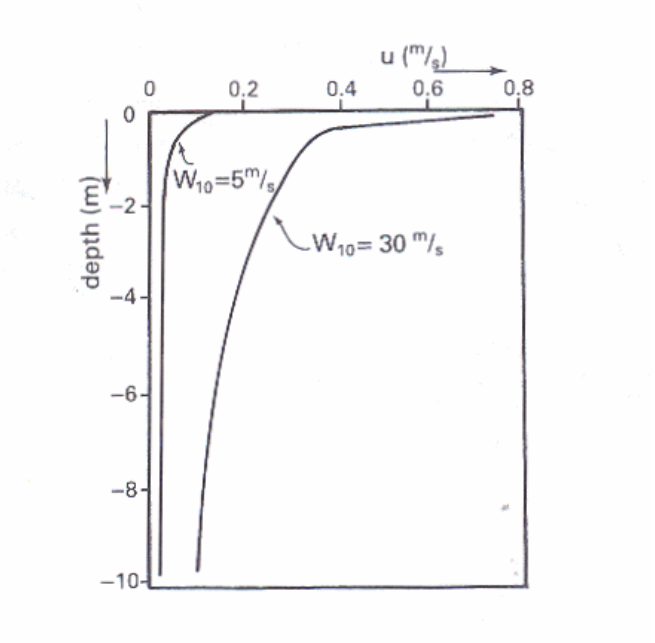

Figure 4.1 *Wind-induced velocity profiles in deep water*

When the wind is blowing in a certain direction in deep water, current velocities will be induced in that direction and due to Coriolis forces also in various other directions. This latter behaviour is known as Ekman turning, see **Figure 4.2**. The Ekman spiral can only be generated in ideal conditions far away from coasts when the wind is blowing sufficiently long in the same direction. Other effects such as density gradients will lead to deviations. In shallow water near the coast the Ekman spiral will be deformed because of the presence of pressure gradients related to water surface variations. In shallow nearshore water (depth smaller than 10 m) the current responds rapidly to wind stresses and the surface current tends to be aligned with the wind direction. The shore-normal component of the surface wind stress causes set-up or set-down at the shore. As a result a shore-normal pressure-gradient is generated yielding an onshore or offshore bottom current, see **Figure 4.3**. Near the shoreline this causes downwelling (downward flow of water) in case of a set-up of the mean sea level at the shore or upwelling (upward flow) in case of set-down.

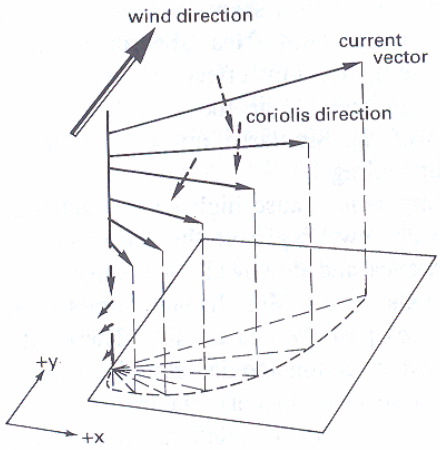

Figure 4.2 *Ekman spiral of velocities*

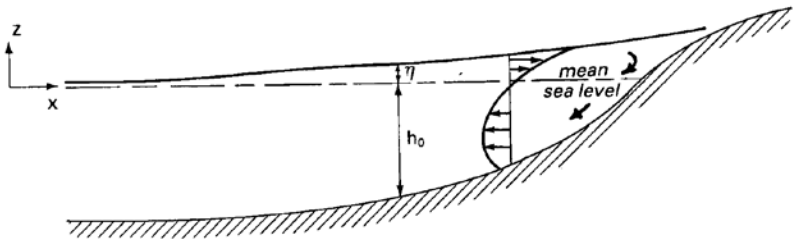

Figure 4.3 *Wind-induced set-up and circulation due to onshore wind*

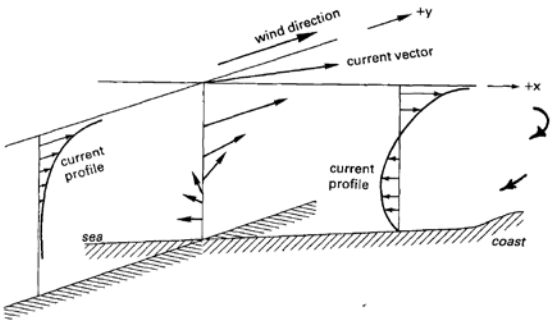

Figure 4.4 *Wind-induced circulation due to longshore wind*

Longshore winds and associated longshore currents also generate cross-shore currents by the action of Coriolis forces yielding a (relatively small) water surface set-up or set-down near the shoreline, depending on wind and Coriolis direction. A pressure gradient balancing the Coriolis force is generated resulting in a circulation pattern with a seaward-directed bottom current in case of a nearshore water surface set-up, see **Figure 4.4**. Near the surface (northern hemisphere) the current vector is turning to the right due the Coriolis effect, whereas it is turning to the left in the bottom region due to the pressure gradient. Near the shoreline the surface fluid is forced downwards which is known as downwelling. Similarly, upward flow of water near the shoreline (in case of a set-down) is known as upwelling.
Storm winds with strong onshore components cause high locally generated waves and onshore-directed surface currents resulting in downwelling over the shoreface (offshore-directed bottom currents). The combination of high waves and downwelling results in relatively large offshore-directed sand transport rates along the shoreface. Most frontal storms produce a rapid shift of the wind as the front or storm center moves past the coastal site. These latter winds have offshore components which work against the wave direction and decrease the wave height. Furthermore, the offshore winds cause offshore-directed surface currents, which may lead to upwelling over the shoreface (onshore-directed bottom currents). More detailed information is given by **Niedoroda and Swift, 1991**.
The coastal zone where the wind-induced currents are affected by Coriolis forces, is known as the geostrophic zone (depths larger than about 25 m).

Analysis of cross-shore current velocities in the near-bed region of shallow coastal zones often shows a systematic longterm onshore or offshore-directed residual current velocity in the range of 0 to 0.05 m/s, which are especially important for the net cross-shore transport rates. Generally, offshore-directed residual current velocities do occur in shallow depths during onshore-directed storm winds. For example, the Egmond data **(Houwman and Hoekstra, 1994)** show offshore-directed near-bed velocities of about 0.15 m/s in the waning phase of a storm (**Figure 6.8**).

Storm surges of several metres high in the nearshore zone can be generated by:

- direct effect of onshore wind forces,
- action of Coriolis forces related to wind-induced longshore currents,
- inverted-barometric effect of low atmospheric pressure in the storm wind field.

Seaward-directed bottom currents associated with storm surges are relatively strong (order of 1 m/s). Significant storm-driven currents will be generated in the shoreface zone during extreme events (major storms, cyclones, hurricanes). Bottom current velocities may be as large as 2 m/s.

Long shelf (barotropic) waves with amplitudes of the order of 0.1 m and lengths of the order of 100 km may be generated by varying longshore wind forces. **Hegge et al (1996)** observed shelf waves with amplitudes of 0.2 to 0.4 m and periods of 5 to 20 days along the west coast of Australia related to the passage of large-scale anticyclonic weather systems. Peak current velocities of long shelf waves are of the order of 0.1 to 0.2 m/s in longshore direction and in phase with the water level elevation.
Field data of mean sea levels in storm conditions in the Belgian and Dutch coastal zone (North sea) are reported by **Groenendijk, 1993**. For conditions with more or less shore-parallel winds of 10 to 15 m/s the mean sea level along the coast showed a difference of 0.1 to 0.2 m over a longshore distance of about 250 km (high level at downwind end).

Wright et al (1986, 1994) deployed instrumented tripods on the shoreface of the Middle Atlantic Bight (M.A.B.) to measure the near-bed current velocities. This area is dominated by storms. The largest waves and strongest currents are generated by extratropical northeasterly storms. Wind-driven near-bed current velocities of 0.3 to 0.5 m/s were observed in longshore and cross-shore direction in depths of 8 and 13 m. Sometimes these

currents are intensified by strong infragravity pulsing. In many cases the seaward pulses of flow coincided with packets of high waves consistent with the model of group-bound long waves. The response time of the near-bed cross-shore velocities to the wind velocities was of the order of 10 hours. The response time of the near-bed longshore velocity was much shorter (3 hours). The local bed response measured by an altimeter attached to a steel pipe driven into the bed, showed vertical variations of about 0.1 to 0.15 m. The rapidity of the bed accretion under the altimeter pointed to the pulse-like migration of a sediment front (bed form migration).

Weishar and Meadows (1987) performed velocity measurements in the M.A.B. offshore of the Duck site during a storm in Sept. 1985. During the growth of the storm the near-bed longshore velocities reversed and attained values of 0.3 m/s at a depth of 13 m. Onshore-directed near-bed current velocities of 0.15 m/s were measured. The response time of the near-bed velocities to the wind velocities was of the order of 24 hours.

5 Density-induced currents

Density-induced currents are related to spatial density gradients of the fluid-sediment mixture due to variations of temperature, salinity and/or sediment concentration.

Density variations induced by temperature effects usually are related to a surface layer consisting of relatively low density (warmer water) and a bottom layer of relatively high density (colder water). The boundary between upper warmer water and the underlying colder water is known as the pycnocline. The component of flow driven by the slope of internal density surfaces is known as the **baroclinic** component, the component of flow driven by the slope of the sea surface is known as the **barotropic** component.

The friction-dominated zones are hardly affected by stratification because of the presence of strong turbulent mixing processes.

Density variations induced by salinity variations are most commonly the result of river (fresh water of relatively low density) outflow in the coastal zone, where the fluid density is relatively large. This will lead to horizontal and vertical circulations. The density-gradient effect is most pronounced in the near-bed region yielding relative large onshore near-bed velocities during the flood tide and relatively small offshore near-bed velocities during the ebb tide. As a result a near-bed residual current (landward) is generated (gravitational circulation), which may cause a net landward transport of sediments. Near the water surface this process is reversed yielding a residual seaward flow, see **Figure 5.1**.

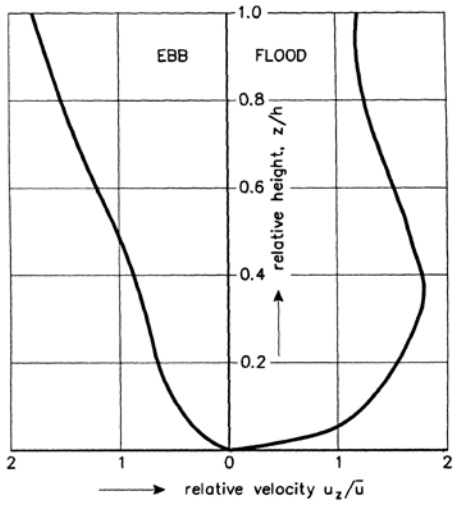

Figure 5.1 *Influence of horizontal density gradient on velocity profile during ebb and flood tide*

An illustrative example of density-induced flow circulation is the fresh water discharge of the Rhine river in the Dutch coastal zone near the harbour of Rotterdam and its effects on the tidal flow system. The behaviour of the salinity and fluid density gradients is strongly related to the magnitude of the Rhine discharge (average of 2200 m^3/s, peak of 10,000 m^3/s). Fluid density variations over a longshore distance of 100 km and a cross-shore distance of 30 km have been observed **(De Ruijter et al, 1992)**. **Figure 5.2** shows salinity patterns in the Noordwijk transect (about 30 km north of the Rhine outlet) for a discharge of 6000 m^3/s. Stratification is extreme during these conditions. During periods of low discharge (1400 m^3/s) the stratification effect is almost absent in the Noordwijk transect, but a horizontal density gradient still exist (see **Figure 5.2**). Residual current velocities based on one-year observations show onshore-directed values of 0.02 to 0.04 m/s in the near-bed region (see **Figure 5.2**). The residual currents in the near-water surface region are dominated by wind and tide effects; net values are directed northward (0.05 to 0.1 m/s).

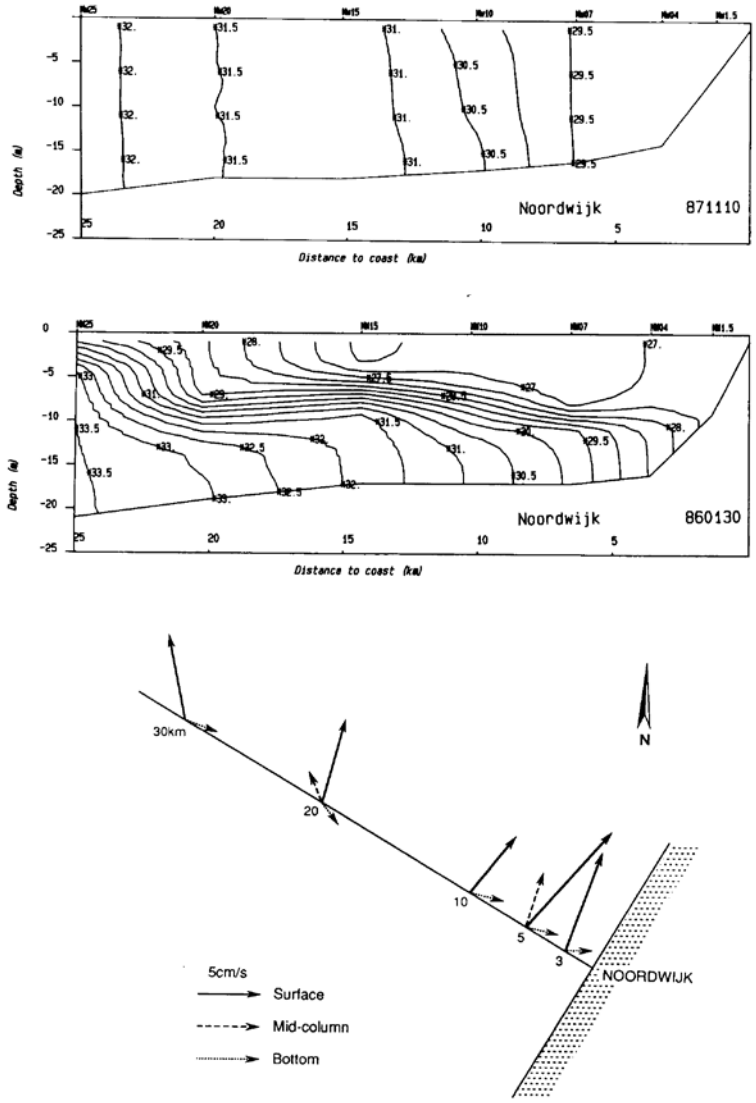

Figure 5.2 *Salinity variations and net annual currents in cross-shore transect Noordwijk at 30 km north of Rhine outlet, (De Ruijter et al, 1992)*
Top: salinity distribution at low discharge of 1400 m^3/s
Middle: salinity distribution at high discharge of 6000 m^3/s
Bottom: net annual currents

6 Wave-induced currents

The wave and current fields interact mutually through a number of mechanisms:

- refraction of the waves by horizontal currents,
- generation of near-bed streaming by the waves,
- generation of longshore currents by breaking waves,
- modification of the wave kinematics by the currents,
- modification of the vertical flow structure by the waves,
- enhancement of the bottom friction felt by the currents due to interaction with the wave boundary layer,
- enhancement of the bed shear-stresses and energy dissipation of the waves due to interaction with the current boundary layer.

6.1 Drift and streaming

Stokes (1847) first pointed out that the fluid particles do not describe exactly closed orbital trajectories in case of small-amplitude sinusoidal surface waves in perfect irrotational (non-viscous) conditions. The fluid particles have a second-order mean Lagrangian velocity (called Stokes-drift) in the direction of wave propagation resulting from the fact that the horizontal orbital velocity increases slightly with distance above the bed. Consequently, a particle at the top of an orbit beneath the wave crest has a greater forward velocity than it has at the bottom of the orbit beneath the wave trough. The depth-integrated mass flux associated with waves propagating in a horizontally unbounded domain is given by $M = gH^2/(8c)$ with H = wave height and c = wave propagation velocity. Assuming a zero mass flux (bounded domain) over the water depth, the onshore mass flux in the upper part of the depth is balanced by a return mass flux in the near-bed region of the water column, see **Figure 6.1**.
As the waves enter shallow water, the orbits become more elliptical and the drift velocities increase to appreciable values (order 0.1 m/s). The mass flux can also be determined in an Eulerian way by integration over time and space of the instantaneous horizontal velocities between the wave trough level and the wave crest level. In this region there is an asymmetry of the horizontal velocity; more fluid moves forward in the crest region than backward in the trough region.
Both methods (Lagrangian and Eulerian) yield the same value of the mass flux, but a different distribution over the depth.
When waves enter a weak current field, Langmuir circulation cells may be generated in the lateral plane (normal to the main flow direction) due to the presence of lateral variations of the Stokes drift.

Longuet-Higgins (1953) has shown that for real fluids with viscosity v there is a time-averaged net downward transfer of momentum into the wave boundary layer by viscous diffusion producing a mean Eulerian streaming in addition to the Stokes drift. Assuming a zero mass flux over the depth, Longuet-Higgins found a vertical distribution as given in **Figure 6.2**. The wave-induced streaming in the boundary layer is onshore directed and of the order of $(U_\delta)^2/c10$ with U_δ = peak orbital velocity at edge of boundary layer and c = wave propagation velocity.

A detailed experimental flume study of wave-induced streaming in non-breaking waves over both plane and sloping bottoms was performed by **Klopman (1994)** using Laser-Doppler velocimetry. Monochromatic and random waves were generated. Active wave absorption boards were used to eliminate wave reflection and resonance. The flume bottom consisted of gravel particles (0.002 m) with an effective Nikuradse roughness of 0.0012 m.

Figures 6.3 and **6.4** show the mean horizontal velocities over a horizontal and a sloping bottom, as measured by Klopman.

In case of monochromatic waves over a horizontal bottom the wave-induced streaming shows maximum values of about 0.01 m/s (approx. 6% of peak orbital velocity of 0.18 m/s) in the wave propagation direction. The thickness of the layer with wave-induced streaming is about 0.02 m which is about 4 times the wave boundary layer thickness. Above the streaming layer a return flow layer balancing the mean mass-flux between the wave trough and crest can be observed.

In case of random waves over a horizontal bottom maximum streaming velocities of about 0.012 m/s can be observed; the thickness of the streaming layer shows a significant increase to about 0.1 m.

In case of monochromatic and random waves (non-breaking) over a plane sloping bottom the maximum streaming velocities are smaller (0.009 to 0.004 m/s). The layer thickness is about 0.01 m which is considerably smaller than that in case of a horizontal bottom.

The experimental results of **Klopman (1994)** confirm the theoretical results of **Longuet-Higgins (1953)** yielding an onshore-directed streaming near the bottom.

In strongly asymmetric (shoaling) waves over steep sloping bottoms the net velocities in the streaming layer may be offshore-directed due to an unbalance of the fluid shear stresses in the wave-boundary layer during the forward and backward phases of the wave cycle.

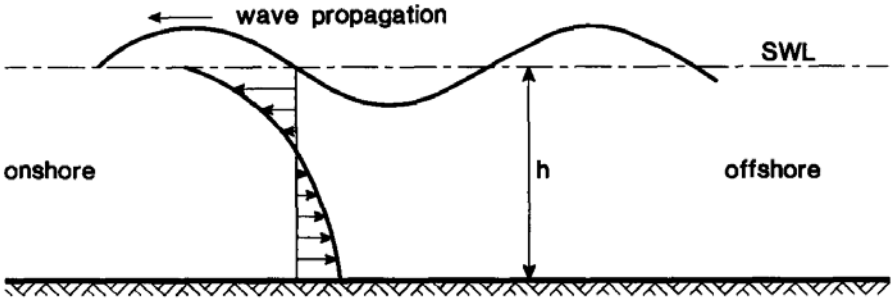

Figure 6.1 *Drift velocity profile according to Stokes*

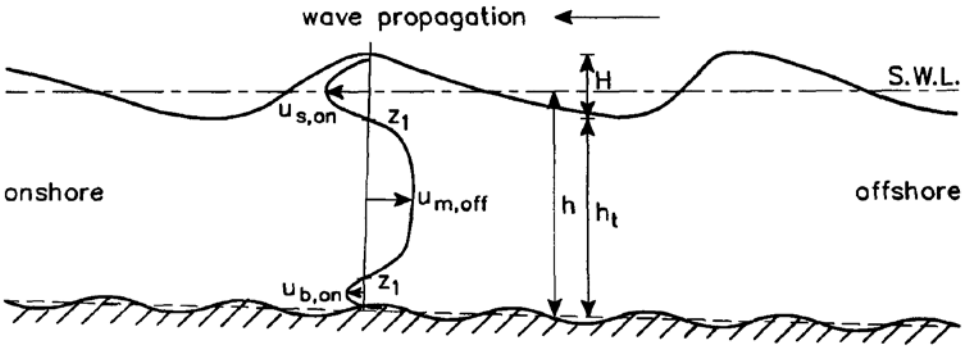

Figure 6.2 *Velocity profiles according to Longuet-Higgins (1953)*

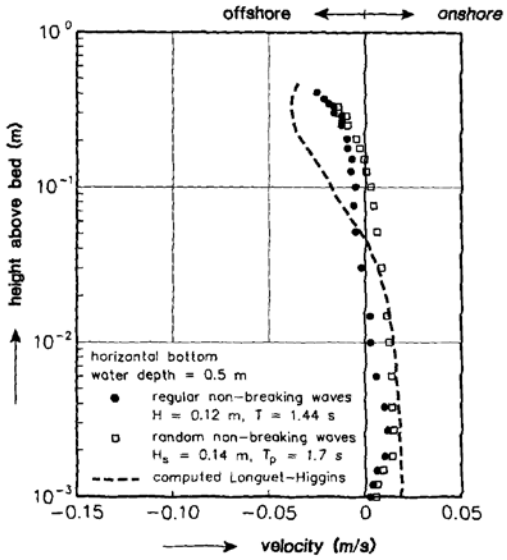

Figure 6.3 *Wave-induced streaming in case of monochromatic and random waves over horizontal bottom*

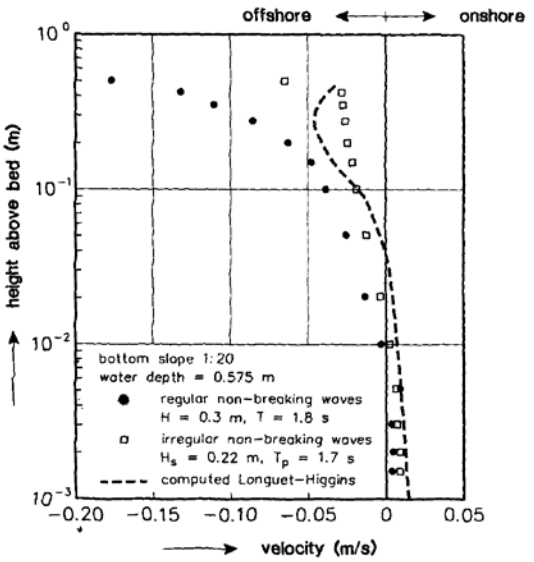

Figure 6.4 *Wave-induced streaming in case of monochromatic and random waves over plane sloping bottom*

6.2 Currents due to breaking waves

Mass transport in the near water surface region is considerably enhanced in breaking wave conditions. When oblique incident waves break in the nearshore zone, a complicated current pattern is generated in the surf zone, consisting of:

- longshore current,
- offshore return current in the near-bed region (undertow).

Figure 6.5 shows the vertical structure of the mean currents in the surf zone **(Svendsen and Lorenz, 1989)**.
The mean currents interact with the instantaneous wave orbital motions yielding a complicated time-dependent three-dimensional pattern.

The generation of the longshore and cross-shore mean currents can be explained by the radiation stress concept which describes the momentum fluxes associated with the waves.
In the surf zone along a uniform coast the decaying incident waves generate an onshore gradient of the onshore component (S_{xx}) and the longshore component (S_{xy}) of the radiation stress, see **Figure 6.6**. The gradient of the onshore radiation stress component is balanced by the pressure gradient related to the mean water surface set-up in the surf zone. As a result of the onshore mass transport in the near surface region and the mean water surface set up, an offshore return current below the trough level is generated, which is known as the undertow, see **Figure 6.7**.
Figure 6.7bottom shows measured undertow velocities for a test performed in SUPERTANK-experiments in the USA **(McKee Smith, 1995)**.
Figure 2.3 shows measured undertow velocities across a breaker bar in a laboratory flume **(Grasmeijer and Sies, 1995)**.

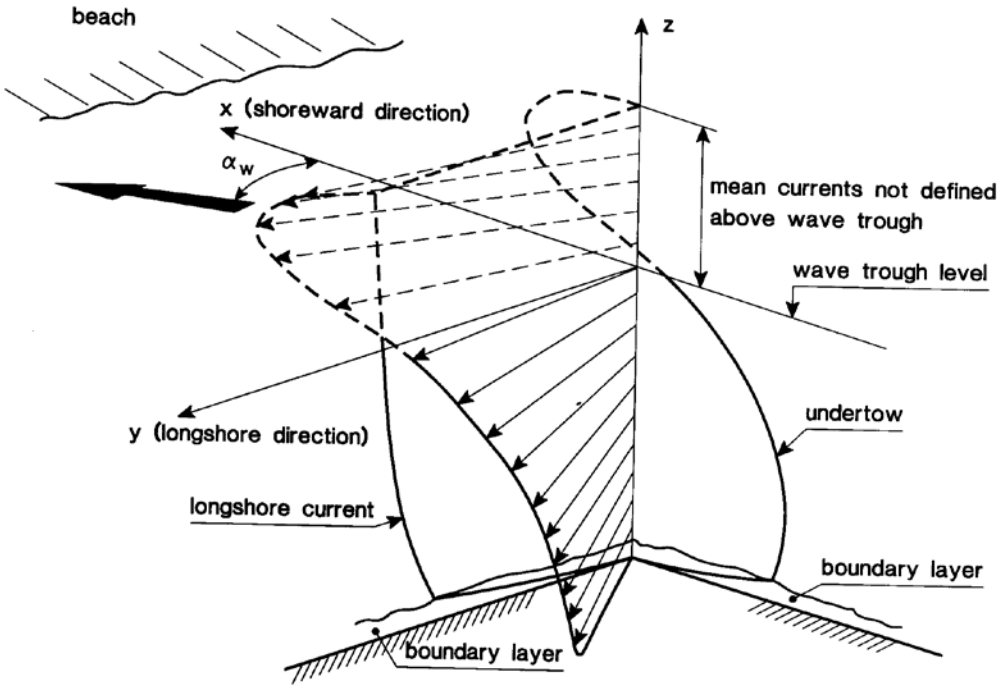

Figure 6.5 *Three-dimensional structure of mean velocities in surf zone (Svendsen and Lorenz, 1989)*

The driving force of the longshore current is the onshore gradient of the longshore radiation stress (S_{xy}) component which is balanced by bottom friction and dispersive shear stresses, see **Figure 6.6**. The longshore current is largely confined to the surf zone, rapidly decreasing in velocity seaward of the breakerline. The longshore velocity is found to be strongly related to the wave height decay in the surf zone and the orientation of the wave crests (angle of wave approach). The beach slope appears to be of less importance. In nature the wave-induced longshore currents are often enhanced by wind-induced currents. Analysis of field data has shown that the cross-shore distribution of the longshore current is rather insensitive to the contributions of individual waves in a random wave field.

Figure 6.8 show examples of mean longshore and cross-shore velocities measured under storm conditions in shallow water in two stations near Egmond along the Dutch Coast **(Houwman and Hoekstra, 1994a)**. The velocities were measured by electromagnetic current sensors mounted in stand-alone tripods at about 0.5 m above the bed. The data in station B-91 (water depth of about 10 m, see **Figure 6.8**) show maximum offshore velocities of 0.2 m/s and maximum longshore velocities of 0.4 m/s. Semi-diurnal tidal effects and wind-induced effects can be clearly observed. The wind enhances the flood current up to t= 70 hours; after that the wind enhances the ebb current.

The data of station S-91 in the surf zone (water depth of about 4 m, see **Figure 6.8**) show considerably larger current velocities. The maximum velocity of the undertow current is about 0.8 m/s. The maximum longshore current is about 1.4 m/s. These values are considerably larger than those in deeper water (see **Figure 6.8**) which are dominated by tide- and wind-effects.

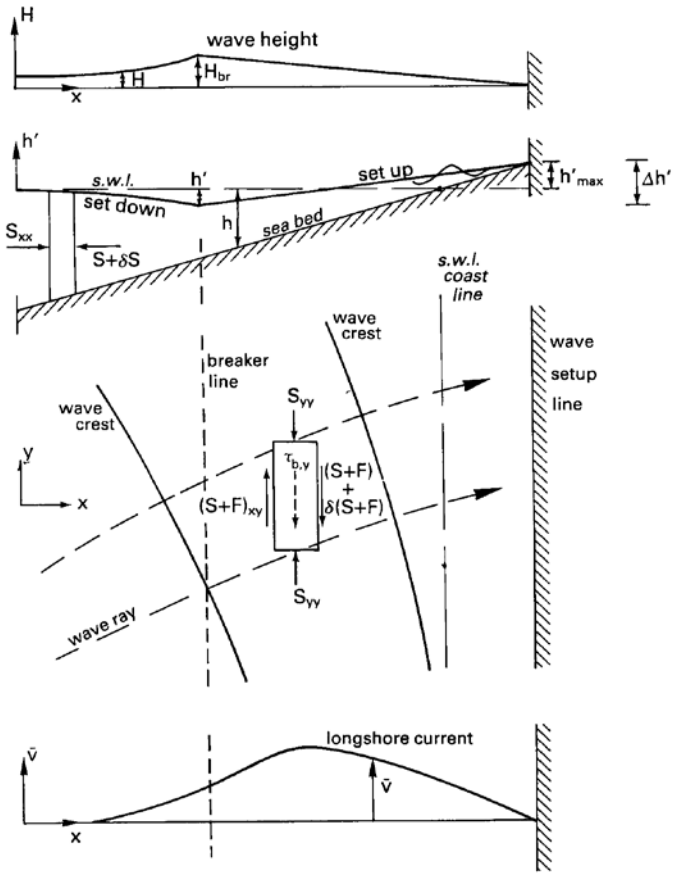

Figure 6.6 *Wave-induced mean water level variations and currents in the surf zone*

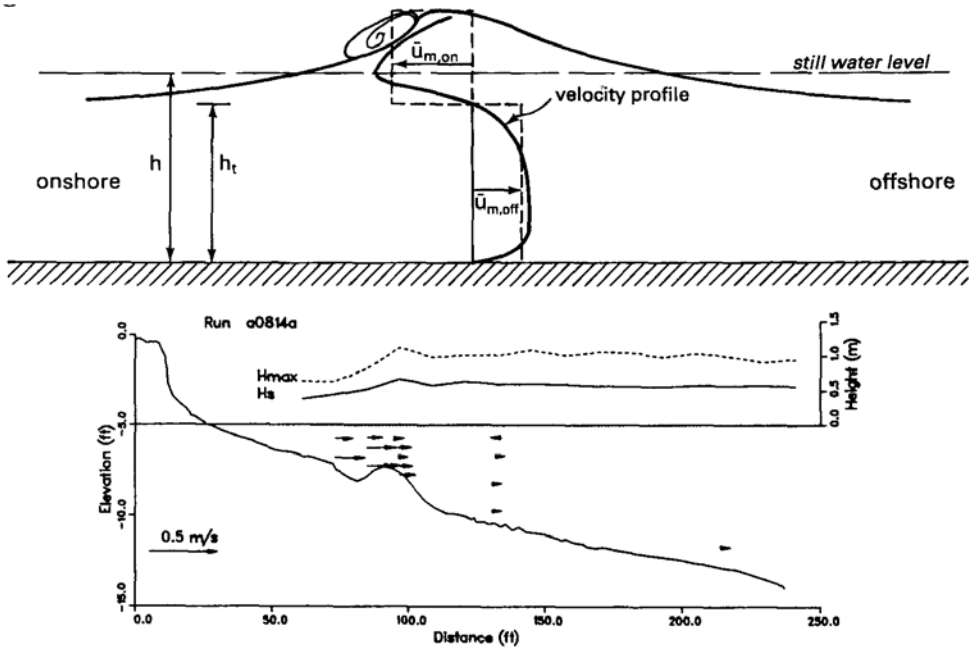

Figure 6.7 *Return currents (undertow) in surf zone*
Top: vertical structure of undertow
Bottom: measured values Supertank-experiment

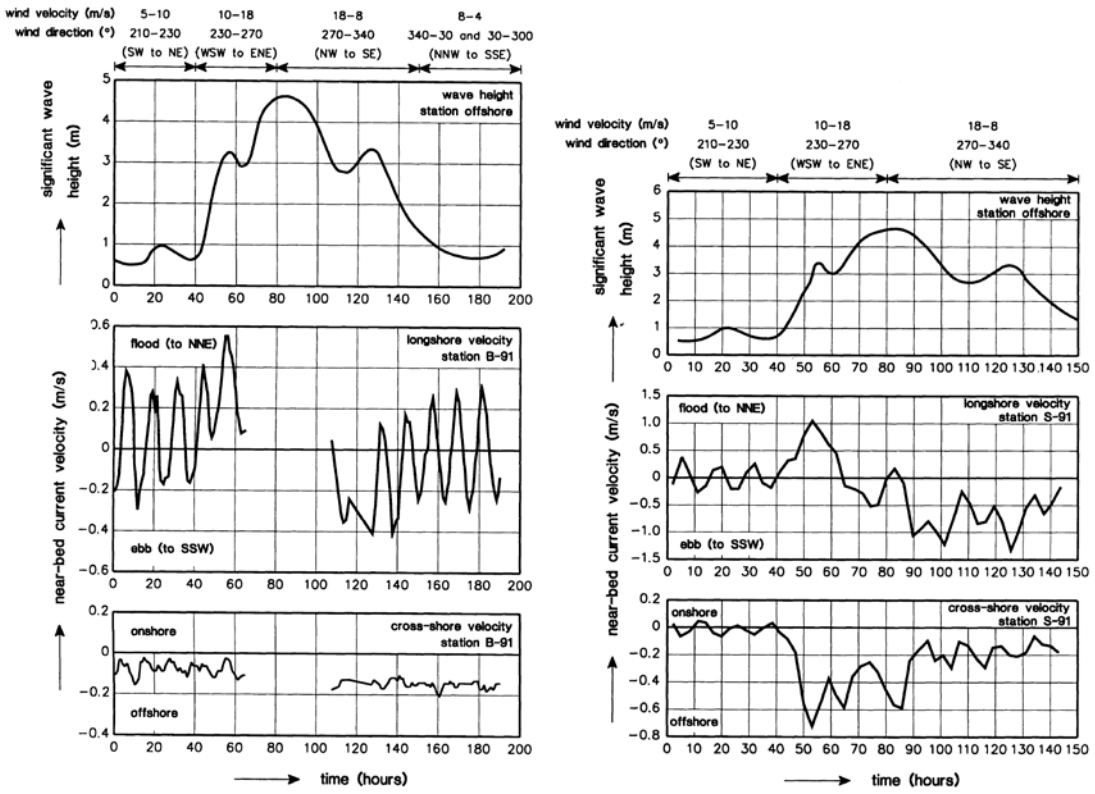

Figure 6.8 *Significant wave height and time-averaged current, The Netherlands*
Left: station B-91 Egmond (depth = 10 m, see Fig. 2.4)
Right: station S-91 Egmond (depth = 4 m, see Fig. 2.4)

Figure 6.9 shows longshore currents for cross-shore profiles with and without breaker bars at beach locations in the USA: Santa Barbara beach 1980 **(Thornton and Guza, 1986)** and Duck beach 1990 **(Church and Thornton, 1992)**.
In the Santa Barbara case (H_{rms}=0.56 m, T_p=14 s, angle=9^0 at a depth of 3.8 m) with a monotonically upsloping bed profile the maximum longshore current velocities do occur in the zone landward of the location of wave breaking (40 m from the shoreline).
In the Duck case (H_{rms}=0.75 m, T_p=11 s, angle=17^0 at a depth of 3.7 m) a relatively small bar was present at a distance of about 75 m from the shoreline. The maximum current velocities can be observed in the trough landward of the bar (x=50 m) whereas wave breaking begins at x=100 m from the shoreline. There seems to be a considerable lag between wave breaking and generation of longshore currents.

This latter effect may be related to:

- non-local energy transfer from breaking waves to kinetic energy of longshore current (lag effect),
- horizontal (cross-shore) mixing and
- longshore gradients in wave set-up related to variations in breaker type (spilling, plunging) and in longshore bar dimensions.

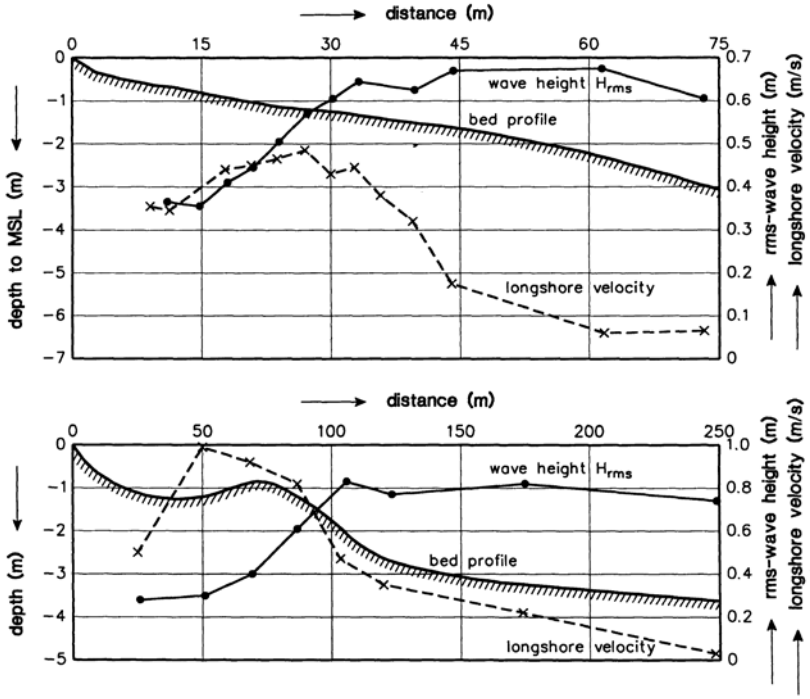

Figure 6.9 *wave-induced longshore currents*
Top: Santa Barbara 4 Feb. 1980 (Thornton and Guza, 1986)
Bottom: Duck 10 Oct. 1990 (Church and Thornton,1992)

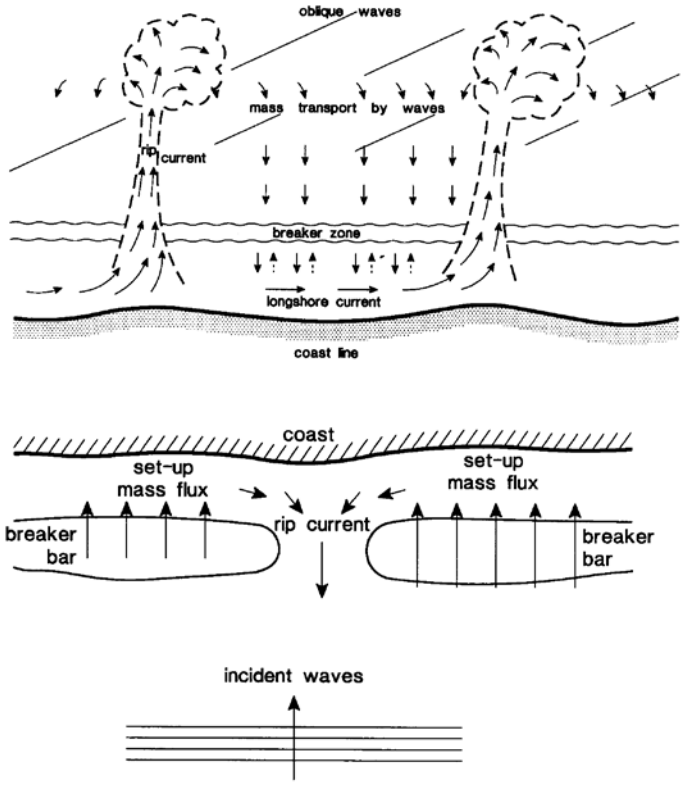

Figure 6.10 *Longshore currents and rip currents (circulation cells)*
Top: principle of rip current generation
Bottom: nearshore circulation cells

The longshore velocities measured in the Duck beach case were modelled by **Van Rijn and Wijnberg (1994)** using a wave by wave approach. Reasonable agreement between measured and computed longshore velocities could only be obtained by introducing a longshore water surface gradient in the inner surf zone.
Longshore currents may be enhanced by longshore variations of set-up caused by variations of the bottom topography (shoals), incident wave heights and/or the type of wave breaking (spilling, plunging). As a result, water may be driven from regions of high waves towards regions of less high waves in the surf zone. The generation of standing edge waves trapped in the surf zone may also produce regular patterns of high and low wave heights along the beach providing a mechanism for regularly spaced circulation cells, especially in steep, reflective beach conditions. Rip currents associated with standing edge waves have a spacing equal to the alongshore wavelength of the edge wave; rips occur at the locations of anti-nodes where amplitudes are relatively small.
Wave trains approaching the beach at different angles (intersecting waves) may also create regular longshore variations of the mean water level and wave height.

Theoretically, there is an alongshore uniform landward transport of water (onshore mass flux) in the upper layers of the water column and a uniform return current (offshore undertow) in the lower layers caused by oblique- and normal-incident waves along a straight, uniform beach. On a natural open coast this process takes place in combination with horizontal circulation consisting of longshore currents and localized seaward-directed rip currents. Rip currents and their causes are discussed by **Dalrymple (1978)**.
Observations along uniform and non-uniform coasts show that the longshore currents are turned seaward at (ir)regular intervals (see **Figure 6.10**), yielding circulation cell systems. Rip currents are relatively strong narrow currents that flow seaward through the surf zone affecting the approaching waves and altering refraction patterns. Rip currents are fed by the longshore currents, whereas the longshore currents are in turn fed by the onshore mass transport due to breaking waves in the surf zone. Breaker bars cause strong wave breaking resulting in onshore mass flux and set-up landward of the bar (see **Figure 6.10**). The circulation cells thus consist of an onshore mass transport of water over the breaker bars, longshore currents in the surf zone and seaward-turning rip currents in the channels between the breaker bars, which spread out into rip heads **(Komar and Oltman-Shay, 1991)**.

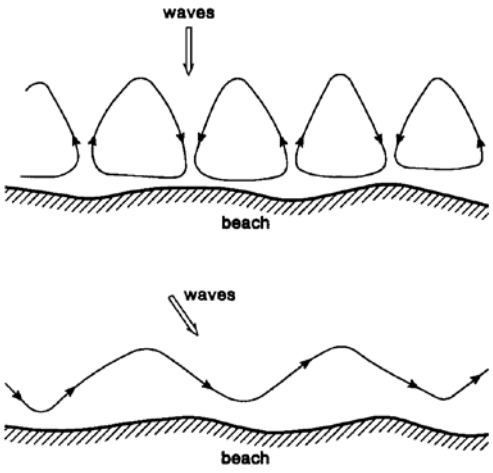

Figure 6.11 *Circulation and meandering patterns in surf zone (after Sonu, 1972)*
Top: circulation under normal-wave incidence
Middle: meander currents under oblique-wave incidence
Bottom: longshore coastline

Along a sandy coast rip currents do occur in the swash zone above MSL and further offshore in depressions (rip channels) between the longshore bars.

Rip currents may also be important in transferring sediment farther offshore well beyond the surf zone (megarips). These megarips or stormrips, which prevail during storms off embayed headland-bounded beaches have velocities of 1 m/s and may extend hundreds of metres beyond the surf zone **(Cowell, 1986)**. Side-scan sonar studies along the Pacific coast of Mexico show shore-normal bands of rippled sediment beds extending from the beach over a distance of 1500 m in water with depths up to 30 m **(Reimnitz et al, 1976)**. In some places channels were scoured below the adjacent seafloor. The areas with ripple zonation were generally found to correspond to areas with pronounced rip-current heads. Rip currents off headlands are the most strongest and extend farthest seaward. The best developed ripple zone was seen off a headland. These features are attributed to storm rips.

Sonu (1972) reported about field observations of rip currents at a site (Seagrove) in Florida, USA. The 30- to 50-meter wide surf zone was shallow; the depth over the inner bar was 1 meter or less. Outside the inner bar the bottom dropped steeply to about 5 meters, and then rose to about 4 meters at the outer bar, approximately 200 meters from the shoreline. The wind waves were generally small (up to 0.5 m) and swell waves were as large as 0.2 m. The breaker height just outside the inner bar was essentially uniform in longshore direction. It was possible to distinguish two major current patterns, depending on the wave-incidence angles. A pattern associated with normal-wave incidence was characterized by a series of discrete circulation cells (longshore diameters of 30 to 60 m), as shown schematically in **Figure 6.11**.
Adjacent cells rotated in opposite directions so that the rip currents, which developed at the confluence of the seaward currents of these cells, were spaced at every two cells. Shoreward currents were of the order of 0.2 to 0.3 m/s, whereas the outflow velocities in the rip attained values as much as 2 m/s. The circulations were of the pulsational type; occasional strong outflows at beat frequencies caused water to escape from the circulation. Circulations were generally stronger during high tide than during low tide. Low rip-current velocities at high tide fluctuated with incoming swells, whereas high velocities at low tide tended to fluctuate at surf beat frequencies. Meandering currents associated with oblique-wave incidence could be explained as a combined effect of circulation cells and parallel longshore flows (see **Figure 6.11**).

Dette et al (1995) measured velocities in a rip channel separating two adjacent bars in the surf zone on the west coast of the island of Sylt in the North sea (Germany), as shown in **Figure 6.12**. Typical spatial scales of the rip channel are width of 50 m and length of 200 m. Tidal ranges in the study area are about 2 m (mesotidal coast). The tide-related velocities in station S3 in the rip channel have typical values of 0.6 m/s (5 minutes averaged) in longshore direction and 0.3 m/s in cross-shore direction. During storm conditions the offshore-directed rip current at location S3 was varying between 1 and 2 m/s for a period of about 20 hours (see Figure 6.12). The longshore velocity component at location S3 showed similar values. Instantaneous velocities at S3 measured over a time span of 300 seconds during the peak of the storm are much larger than the 5 minutes-averaged values (see Figure 6.12). In offshore direction the maximum instantaneous velocity was almost 4 m/s as a result of the oscillatory and mean velocity components. The maximum instantaneous velocity in longshore direction was about 4 m/s.

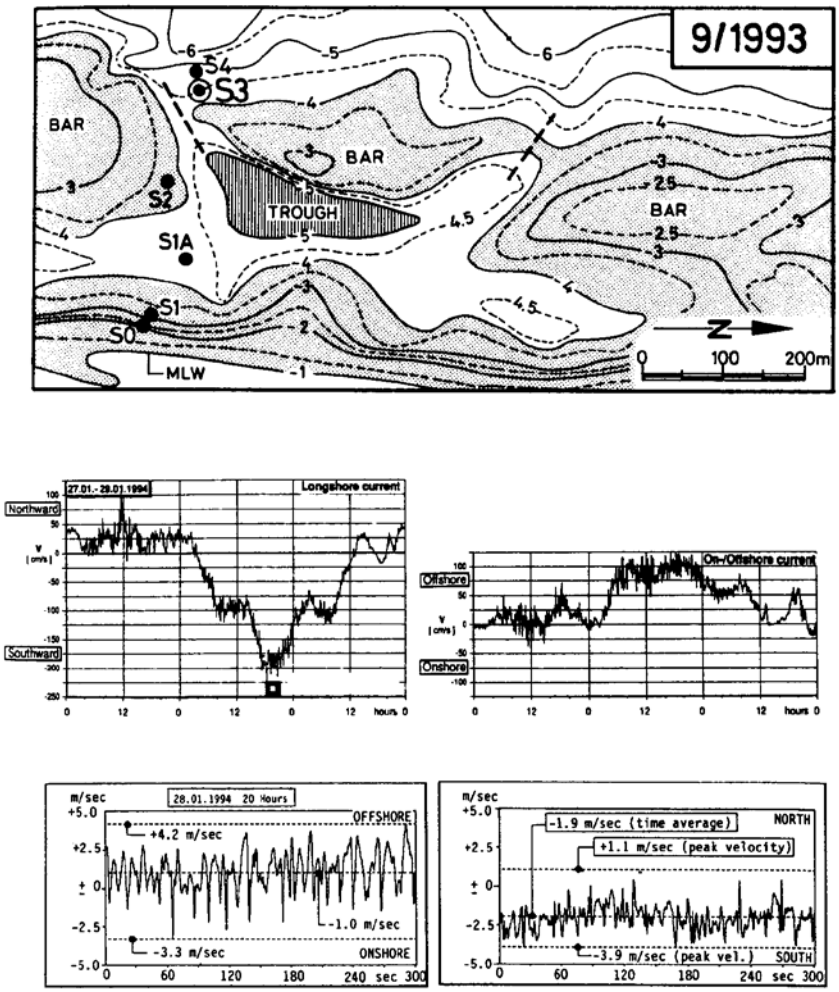

Figure 6.12 *Rip currents near island of Sylt (after Dette et al, 1995)*
Top: location of rip channel
Middle: time-mean current velocities
Bottom: instantaneous current velocities

Aagaard et al (1997) have shown that nearshore rip currents in shallow depths between 1 and 1.5 m at the mesotidal beach at Skallingen (Denmark) are relatively large (up to 0.6 m/s) at low tide, when wave breaking is maximum (H_s/h= 0.35 to 0.4). Long-period fluctuations of 5 to 10 min were observed in the rip current velocities. The measured rip current velocities were found to be in good agreement with predicted values based on $v_{rip}=q_{on}\,\lambda/A$ with q_{on}=onshore mass transport between rips, λ= rip spacing, A= cross-sectional area of rip channel.

Chandramohan et al (1997) studied rip currents along the Goa coast (south of Bombay) of India. This coast consists of sand beaches, sea cliffs, promontories, pocket beaches, dunes and hard rock wave cut platforms. Sea conditions are generally rough during the southwest monsoon (June to September). The foreshore is quite steep; the -5 m line is at 50 to 150 m from the shoreline. The surf zone width is narrow with values of 20 to 80 m during the monsoon period. Longshore currents (dye displacement over 2 min) and rip current spacing were determined at various (15 to 20) stations along a coastal section of about 100 km. The longshore currents generally varied between 0.5 and 0.7 m/s during conditions with breaking wave heights between 0.3 and 0.7 m (periods of 4 to 9 s). The rip spacing was found to be about 300±150 m for all stations.

6.3 Modification of vertical flow structure

The vertical structure of the flow is significantly modified by the wave motions, as shown by many laboratory experiments **(Kemp and Simons, 1982, 1983; Van Rijn et al, 1993; Van Rijn and Havinga, 1995)**.

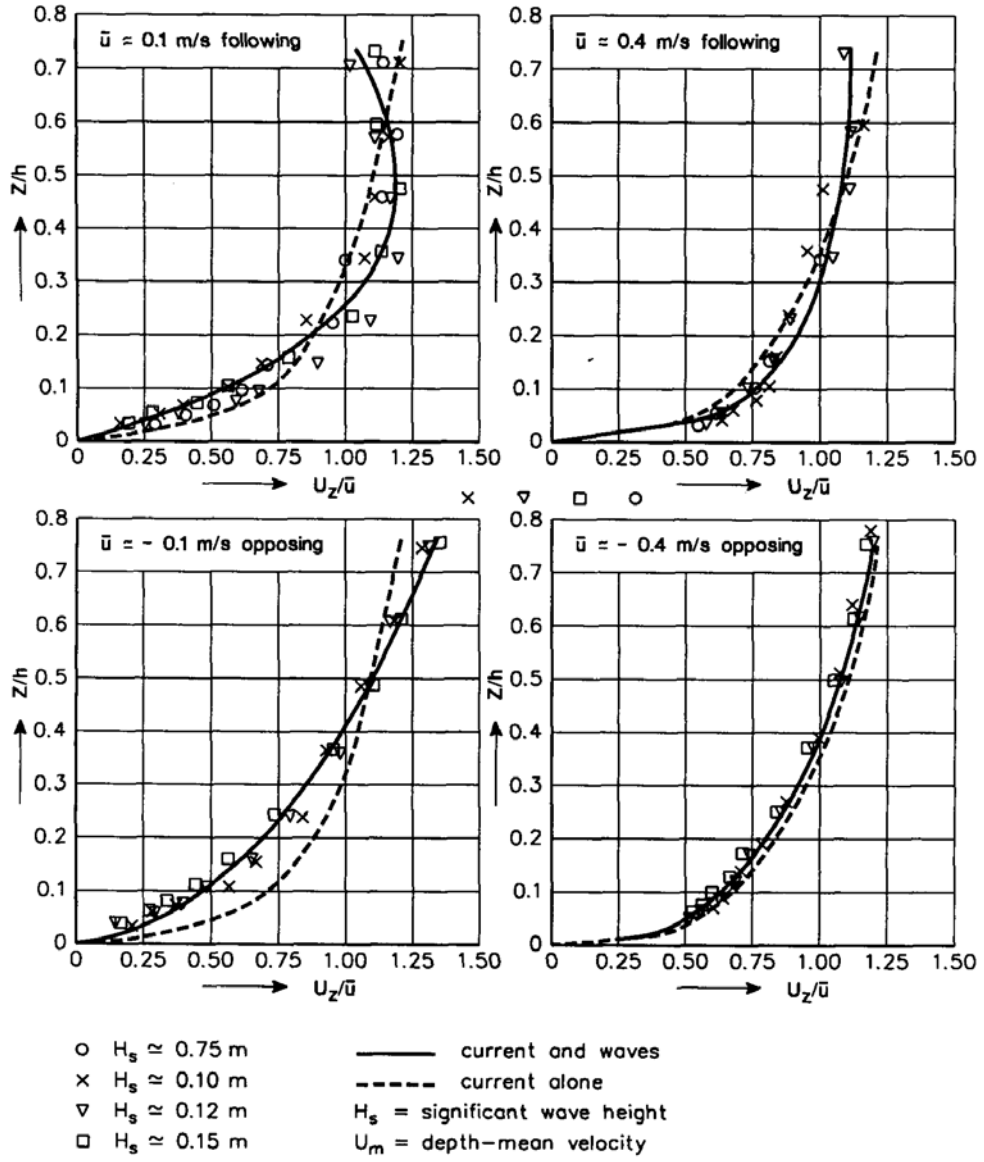

Figure 6.13 *Influence of waves on current velocity profile (Van Rijn et al, 1993) (- opposing current, + following current)*

The current velocities in the near-bed region are reduced by the wave-induced vortices generated in the wave boundary layer (see Figure 6.13), which can be modelled as an apparent bed roughness effect **(Van Rijn, 1993)**. The reduction of the near-bed velocities is most pronounced in case of a weak current combined with high waves. In case of an opposing current the reduction of the near-bed velocities is somewhat larger than in case of a following current. When the wave direction is perpendicular to the current direction, the reduction of the near-bed velocities was found to be largest based on experiments in a laboratory basin with a rippled bed **(Van Rijn and Havinga, 1995)**. The current velocities in the upper layers show an increase in case of waves opposing the current and in case of waves perpendicular to the current. When the waves are in the same direction as the current (following), the velocities near the surface are reduced.

The near-bed boundary layers associated with the waves and the current interact nonlinearly, because they are dominated by turbulent stresses and turbulence generation is a nonlinear phenomenon. This has the effect of enhancing both the mean and oscillatory shear-stresses (see Figure 6.14). In addition, the current profile is modified, because the extra turbulence generated close to the bed by the waves appears to the current as being equivalent to an enhanced bottom roughness. Many mathematical models have been put forward to describe the wave-current interaction **(Soulsby et al, 1993)**. For sediment transport purposes it is important to predict the time-mean bed shear-stress (τ_m) and the maximum bed shear-stress (τ_{max}) in the combined wave-current flow. The entrainment of sediment particles is determined by τ_{max} while the current velocity and the diffusion of suspended sediment into the upper part of the flow are determined by τ_m.

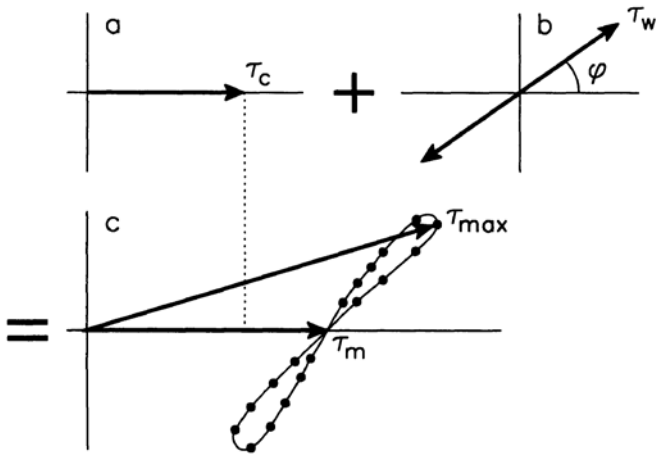

Figure 6.14 *Schematic representation of bed-shear stresses*

7 References

Aagaard, T. et al., 1997a. *Suspended sediment transport and morphological evolution on an intertidal beach. Coastal Dynamics, Plymouth, England*

Beach, R.A. and Sternberg, R.W., 1987. *The influence of infragravity motions on suspended sediment transport in the inner surf zone. Coastal Sediments. New Orleans, USA, p. 913-928*

Chandramohan, P. et al., 1997. *Rip current zones along beaches in Goa, west coast of India, p. 322-327. Journal of Waterways, Port, Coastal, and Ocean Engineering, Vol. 123, No.6*

Church, J.C. and Thornton, E.B., 1992. *Bottom stress modification by breaking waves within a longshore current model. 23rd ICCE, Venice, Italy.*

Cowell, P.J., 1986. *Australian megarip study. EOS 67, p. 449*

Dalrymple, R.A., 1978. *Rip currents and their causes, p. 1414-1427. 16th ICCE Hamburg, Germany*

De Ruijter, W.P.M., Van der Giessen, A., and Groenendijk, F.C., 1992. *Current and density structure in the Netherlands coastal zone. In: Dynamics and exchanges in estuaries and in coastal zone, edited by D. Prandle, American Geophysical Union.*

Dette, H.H., Peters, K. and Spingat, F., 1995. *About rip currents at a mesotidal coast. Coastal Dynamics, Gdansk, Poland, p. 477-488*

Grasmeijer, B. and Sies, R., 1995. *Sediment concentrations and transport in case of irregular breaking waves, Part H and I. Coastal Eng. Dep., Delft Univ. of Technology, Delft, The Netherlands*

Groenendijk, F., 1993. *Long term pressure gradients along the Belgian and Dutch coast. Report DGW-93.045, Nat. Inst. for Coastal and Marine Management, The Haque, The Netherlands*

Groenendijk, F., 1994. *Validation of WAQUA-computations (in Dutch). Note RIKZ/OS-94.111, Rijkswaterstaat, The Netherlands.*

Hamm, L., Madsen, P.A. and Peregrine, D.H., 1993. *Wave transformation in the nearshore zone: a review. Coastal Engineering, Vol. 21, p. 5-39.*

Hegge, B., Eliot, I. and Hsu, J., 1996. *Sheltered sandy beaches of Southwestern Australia, p 748-760. Journal of Coastal Research, Vol.12, No. 3*

Houwman, K.T. and Hoekstra, P., 1994. *Shoreface hydrodynamics; Report part 1, field measurements near Egmond aan Zee. Imau, R94-2, Univ. of Utrecht, The Netherlands.*

Houwman, K.T. and Hoekstra, P., 1994. *Shoreface sediment dynamics; Report part 2, Field measurements near Egmond aan Zee, Imau R94-3, Univ. of Utrecht, Utrecht, The Netherlands.*

Huntley, D.A. et al., 1993. *Long waves and sediment movement on beaches: recent observations and implications for modelling, p. 215-229. Journal of Coastal Research, SI 15*

Kemp, P.H. and Simons, R.R., 1982, 1983. *The interaction between waves and a turbulent current. Journal of Fluid Mechanics, Vol. 116, p. 227-250, Vol. 130, p. 73-89*

Klopman, G., 1994. *Vertical structure of flow due to waves and currents. Report H 840.30, part I and II, Delft Hydraulics, Delft, The Netherlands.*

Komar, P.D. and Oltman-Shay, J., 1991. *Nearshore Currents. In: Handbook of Coastal and Ocean Engineering, Vol. 2, edited by J.B. Herbich, Gulf Publishing Company.*

Kroon, A., 1994. *Sediment transport and morphodynamics of the beach and nearshore zone near Egmond, The Netherlands. Doctoral Thesis, Dep. of Physical Geography, University of Utrecht, The Netherlands.*

Lippmann, T.C., Holman, R.D. and Bowen, A.J., 1997. *Generation of edge waves in shallow water. Journal of Geophysical Research, Vol. 102, No. C4, p. 8663-8680.*

Longuet-Higgins, M.S., 1953. *Mass transport in water waves. Royal Society Phil. Trans., London, Vol. 245, A903, p. 535-581.*

Longuet-Higgins, M.S. and Stewart, R.W., 1964. *Radiation stresses in water waves: a physical discussion with applications. Deep Sea Research, 11, p. 529-562.*

McKee Smith, J., 1995. *Undertow at Superduck. Coastal Dynamics, Gdansk, Poland*

Nelson, R.C., 1983. *Wave heights in depth-limited conditions. Sixth Australian Conf. on Coastal and Ocean Engineering.*

Niedoroda, A.W. and Swift, D.J.P., 1991. *Shoreface Processes. In: Handbook of Coastal and Ocean Engineering, Vol. 2, edited by J.B. Herbich, Gulf Publishing Company.*

Reimnitz, E.L. et al, 1976. *Possible rip current origin for bottom ripple zones to 30 m depth. Geology, Vol. 4, p. 395-400*

Rienecker, M.M. and Fenton, J.D., 1981. *A Fourier approximation method for steady water waves. Journal Fluid Mechanics, 104, p. 119-137*

Roelvink, J.A., 1993. *Surf beat and its effect on cross-shore profiles. Ph.D. Thesis, Dep. of Civil Eng., Delft Univ. of Technology, Delft, The Netherlands.*

Ruessink, B.G., 1995. *On the origin of infragravity waves in the surf zone of a dissipative multiple bar system. Coastal dynamics, Gdansk, Poland*

Ruessink, B.G., 1998. *Infragravity waves in a dissipative multiple bar system. Doc. Thesis, Dep. of Physical Geography, Univ. of Utrecht, The Netherlands*

Sato, S, Ozaki, M. and Shibayama, T., 1990. *Breaking conditions of composite and random waves. Coastal Engineering in Japan, Vol. 33, No. 2.*

Sobey, R.J. and Bando, K., 1991. *Variations on higher-order shoaling. Journal of Waterway, Port, Coastal and Ocean Eng., ASCE, 117 (4), p. 348-368*

Sonu, C.J., 1972. *Field observation of nearshore circulation and meandering currents. Journal of Geophysical Research. Vol. 77, No 18, p. 3232-3247*

Soulsby, R.L. et al., 1993. *Wave-current interaction within and outside the bottom boundary layer. Coastal Engineering, 21, p. 41-69*

Stokes, G.G., 1847. *On the theory of oscillatory waves. Trans. Cambridge, Phil.Soc., Vol. 8, p. 441-455.*

Svendsen, I.A., 1984. *Wave heights and set-up in surf zone. Coastal Eng., 8, p. 303-329*

Svendsen, I.A., 1984. *Mass flux and undertow in surf zone. Coastal Eng., 8, p. 347-365*

Svendsen, I.A. and Lorenz, R.S., 1989. *Velocities in combined undertow and longshore currents. Coastal Engineering, Vol. 13, p. 55-79*

Swart, D.H. and Loubser, C.C., 1978. *Vocoidal theory for all non-breaking waves. 16th ICCE, Hamburg, Germany, p. 467-486.*

Swart, D.H. and Crowley, J.B., 1988. *Generalized wave theory for a sloping bottom. 21st ICCE, Malaga, Spain, p. 181-203.*

Symonds, G., Huntley, D.A. and Bowen, A.J., 1982. *Two-dimensional surf beat; long wave generation by a time-varying break point. Journal of Geophysical Research, Vol. 87, No. C1, p. 492-498*

Thornton, E.B. and Guza, R.T., 1986. *Surf zone longshore currents and random waves: field data and models. Journal of Physical Oceanography, Vol. 16, p. 1165-1178*

Van de Meene, J.W.H., 1994. *The shoreface-connected ridges along the central Dutch coast. Ph.D. Thesis, Dep. of Physical Geography, Univ. of Utrecht, The Netherlands.*

Van Rijn, L.C., 1993. *Principles of sediment transport in rivers, estuaries and coastal seas. Aqua Publications, Amsterdam, The Netherlands.*

Van Rijn, L.C. et al., 1993. *Transport of fine sands by currents and waves, part 1. Journal of Waterways, Port, Coastal and Ocean Engineering, ASCE, Vol. 119, No. 2, p. 123–143.*

Van Rijn, L.C. and Havinga, F., 1995. *Transport of fine sands by currents and waves, part 2. Journal of Waterways, Port, Coastal and Ocean Engineering, ASCE, No. 3.*

Van Rijn, L.C. and Wijnberg, K.M., 1994. *One dimensional modelling of individual waves and wave-induced longshore currents in the surf zone. Report R94-09, Dep. of Phys. Geography, Univ. of Utrecht, The Netherlands*

Van Rijn, L.C. and Wijnberg, K.M., 1996. *One-dimensional modelling of individual waves and wave-induced longshore curents in the surf zone. Coastal Engineering, Vol. 28, p. 121-145*

Weggel, J.R. et al. 1987. *A comparison of the performance of three types of groins. Coastal, Port Engineering Conference of Dev. Countries, Beijing, China*

Weishar, L.L. and Meadows, G.A., 1987. *Suspended sediment concentrations outside the surf zone, Duck85, Coastal Sediments. New Orleans, USA, p. 897-912*

Wright, L.D. et al., 1986. *Response of the mid shoreface of the Southern Mid-Atlantic Bight to a Northeaster. Geo-Mar. Letters 6, p. 153-160*

Wright, L.D. et al., 1994. *Inner continental shelf transport processes: The Middle Atlantic Bight. Coastal Dynamics. Barcelona, Spain, p. 867-877*